ADAPTIVE REMEDIAL ACTION SCHEMES FOR TRANSIENT INSTABILITY

By

YI ZHANG

A dissertation submitted in partial fulfillment of
the requirements for the degree of

DOCTOR OF PHILOSOPHY

ELECTRICAL ENGINEERING

WASHINGTON STATE UNIVERSITY

School of Electrical Engineering and Computer Science

DECEMBER 2007

To the Faculty of Washington State University:

The members of the Committee appointed to examine the dissertation of YI ZHANG find it satisfactory and recommended that it be accepted.

_____

Chair

_____

_____

ACKNOWLEDGEMENTS

The author expresses his deepest gratitude to his advisor, Professor Kevin Tomsovic, for his constructive guidance, fruitful discussions and encouragement throughout this work. The valuable discussions with Professor Vaithianathan Venkatasubramanian and Professor Anjan Bose are also greatly appreciated.

It is gratefully acknowledged that this work was supported in part through the Consortium for Electric Reliability Technology Solutions (CERTS), funded by the Assistant Secretary of Energy Efficiency and Renewable Energy, Office of Distributed Energy and Electricity Reliability, Transmission Reliability Program of the U.S. Department of Energy under Interagency Agreement No. DE-AI-99EE35075 with the National Science Foundation, and in part through PSerc a National Science Foundation I/UCRC.

Finally, the author wishes to thank all the colleagues at the School of Electrical Engineering and Computer Science, Washington State University, especially the power system group, for cooperation and the comfortable working environment.

ADAPTIVE REMEDIAL ACTION SCHEMES FOR TRANSIENT INSTABILITY

Abstract

By Yi Zhang, Ph.D.
Washington State University
December 2007

Chair: Kevin Tomsovic

Remedial action schemes (RAS) are designed to avoid wide spread outages after a severe contingency in the power system. RAS have also been installed to increase the operational transfer capability (OTC) with the restrictions on the transmission expansion in the power systems. In current practice, these schemes are predetermined based on extensive repeated time domain simulations. This dissertation presents an adaptive method for RAS computation. Given a two-area system model and a mode of disturbance (MOD) that the system will separate after a severe fault on the ties, the presented method separately calculates differential potential energy (*DPE*) and residual kinetic energy (*RKE*) with respect to an intermediary case. A sufficient RAS is determined by comparing the *RKE* and the *DPE*. Because the *DPE* can be reused for the new unstable cases, the repeated time domain simulation can be avoided in RAS calculation. This method is adaptive to different operating points and fault locations; it is also can change with different fault clearing times and/or RAS initiation time. This method presents a way to reduce the time domain simulations in the RAS off-line calculation. This method also enables us to establish an adaptive RAS using fast on-line computation.

To support the adaptive scheme, a new transient energy calculation method is proposed based on the curve of equivalent power versus equivalent angle (EPEA curve)

of the power system, which is derived from the concept of corrected kinetic energy. It is particularly suitable for transient energy calculation in situations with varying mechanical power, such as generation rejection.

This dissertation also proposes a concept using the transient instability detection as the trigger of the adaptive RAS. With Phasor Measurement Units (PMU) measurements as input, a decision tree technique is applied to detect system transient instability. MOD information is included in the classifications of the decision trees so that it can be applied for the MOD specific RAS. The effects of the time delay and the synchronization of the PMU sampling, which are independent of the occurrence of the system events, are investigated. Also studied are the effects of different locations of PMU and different input features of the decision trees, such as phasor angle and magnitude, pre-fault transfer power, and discrete system events. IEEE 39-bus and WECC 179-bus systems are used to illustrate and evaluate the proposed methods.

TABLE OF CONTENTS

LIST OF TABLES

LIST OF FIGURES

ACRONYMS

ANN – Artificial Neuron Network

COA – Center of Angles

CUEP – Controlling Unstable Equilibrium Point

DPE – Differential Potential Energy

DT – Decision Tree

EPEA curve – Curve of Equivalent Power versus Equivalent Angle

EM – Energy Margin

GPS -- Global Positioning System

IS – Intelligent System

ISO – Independent System Operator

MOD – Mode of Disturbance

OMIB – One Machine Infinite Bus

OTC – Operational Transfer Capability

PEBS – Potential Energy Boundary Surface

PMU – Phasor Measurement Unit

RAS – Remedial Action Schemes

RKE – Residual Kinetic Energy

SPS – System Protection Schemes

WECC – Western Electricity Coordinating Council

Chapter 1

INTRODUCTION

1.1 Definition of Remedial Action Schemes

1.1.1 Background of RAS

Today, many once separated power systems have been interconnected through AC and/or DC transmission lines. Interconnections of these separate systems have many advantages to individual systems [1], such as sharing the reserves both during normal and emergency conditions, dividing the task of frequency regulation among all the generators of the interconnected systems and so on. Moreover, large amounts of electrical power can be delivered from remote generation locations to load centers over long transmission lines. Although justified economically, long interconnections create particularly difficult problems for reliability. For example, following a severe contingency on a key transmission path, a power system could be vulnerable to transient instability and separate into two groups along this path within the first swing. In some systems, there may be inter-area oscillations between groups of machines interconnected by weak tie lines.

Meanwhile, building new power plants and transmission lines becomes more difficult because of environmental and other restrictions; however, demand continues to

grow. This pushes the power system to operate closer to the stability limits. In a case of severe contingency, the system may collapse and cause blackouts or interruption of the supply for major customers. Recent examples include the 1996 WECC blackout and 2003 Midwest and Northeast U.S. blackout. The cost of supply interruptions is extremely high and major effort is directed at preventing wide area disturbances. Protective actions at the system level are necessary even in situations where no power equipment is subject to be immediate damage.

Preventive control reschedules generation, or takes other appropriate actions, when there is a potential instability in the power system. Security constrained re-dispatch has been used in preventive control. For example, the condition of the Potential Energy Boundary Surface (PEBS) crossing is added to the constraint set in [2] where a nonlinear optimization model is used to reschedule the system. Similarly, in [3] the sensitivity of energy margin is used in the constraint set of an optimization model. In [4], an iterative procedure is implemented between the OPF (optimal power flow) model and the stability assessment by SIME (Single Machine Equivalent) method. The coherency index is used in [5] to measure stability and then rescheduling is calculated by a sensitivity of this index with respect to generation outputs. The problem with preventive control, of course, is that regardless of whether a contingency occurs, or is likely to occur, economic operation of the system is impacted. Under deregulation, preventive control may be a particularly expensive approach to avoid instability and difficult to justify to ma*RKE*t participants.

Alternatively, utilities can use corrective control to maintain system stability. The corrective control is initiated only after a contingency occurs and can benefit the utilities by saving the cost of pre-contingency mitigations. Corrective control is clearly more

attractive in a deregulated environment. The control action can be generation tripping, load shedding, SVC insertion, etc. For severe contingencies, it is a difficult task to decide and initiate a corrective control action, given the extremely short time available for response, so that many utilities implement so-called Remedial Action Schemes (RAS) or System Protection Schemes (SPS), which rely on off-line calculations and fast real time communication and control. RAS has been utilized extensively in the power systems around the world. It not only protects the system integrity following the severe contingencies, but also is used to increase the operational transfer capability (OTC) on the protected transmission path, especially in the situation when the system load level is high and requires greater import of electrical power.

1.1.2 Definition of RAS

As defined in [6], a RAS is designed to detect abnormal system conditions and take predetermined corrective action to preserve system integrity and provide acceptable system performance. A RAS may involve extreme actions such as, generation tripping or load shedding, or less disruptive actions such as, capacitor insertion or transformer tap blocking. The requirements on RAS can be identified as the necessary actions to satisfy the system performance criteria. A RAS control action may be closed-loop or open-loop. Figure 1.1 shows the general structure of remedial action scheme [6]:

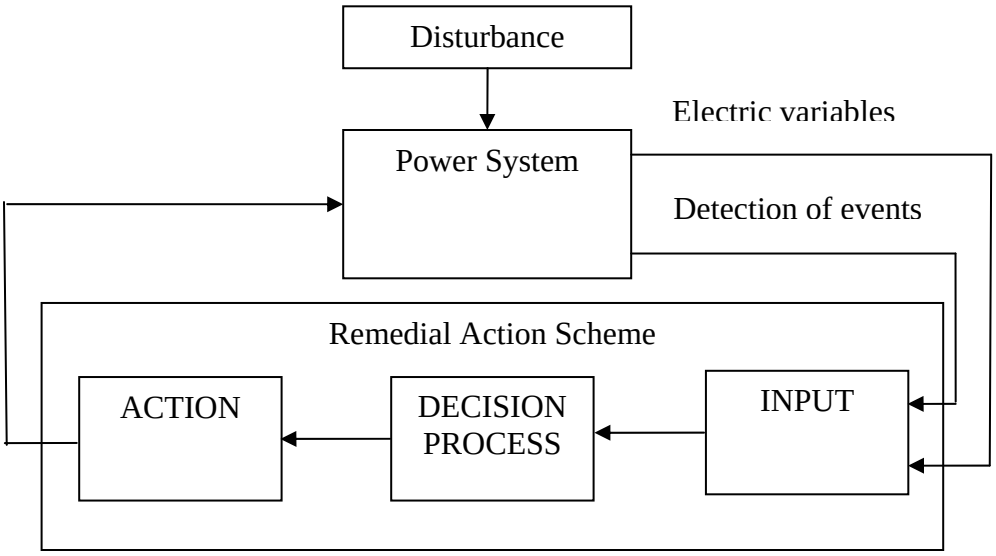

Figure 1.1 General structure of a RAS

RAS tend to be system and situation specific, i.e., each scheme is the dedicated solution for a particular situation in a particular power system, often for specific faults or for specific MOD.

1.2 Overview of RAS Design

1.2.1 General principles

As a system level protective scheme, the RAS design must satisfy the reliability requirements [6]:

- Dependability: a measure of certainty to operate when required.
- Security: a measure of certainty that RAS will not operate when not required.
- Selectivity: the ability to affect the least amount of action when performing its intended function.

- Robustness: the ability to work correctly over the full range of expected steady state and dynamic system conditions.
- Coordination with other protective actions, including other RAS and conventional protection and controls.
- The consequence resulting from a failure of the RAS.

1.2.2 Inputs to RAS

The inputs to a RAS can involve discrete system events and/or continuous electrical variables as shown in Figure 1.1. Depending on the control variables and the method of the instability detection, existing RAS can be classified as event-based or response-based. Event-based RAS are designed to operate on the recognition of a particular combination of events (such as loss of several tie lines between two areas) [6]. An event-based RAS can be faster since it need not wait for the development of the system responses. Examples of event-based RAS are generation rejection and/or load shedding initiated by transmission line tripping. Generally, event-based RAS belongs to the class of open-loop controls. On the other hand, response-based RAS are based on real-time measurements and initiate the control actions when the responses hit some trigger level. A response-based RAS is mainly for slow phenomena, but can operate for unknown events and varying operating scenarios. Response-based RAS can be implemented as a feedback control, for example, wide area signals can be provided to the governors or PSS of some generators to increase system damping when the oscillation occurs in the system.

In current practice, to protect the system from transient instability, event-based RAS are utilized given the extremely short time for response. Considering the complexity of the power system operation, it is still desired to trigger the RAS based on both system

events and its consequent responses. For example, in the design principles of Hydro-Quebec's defense plan [7], it is suggested to detect the consequences of contingencies, rather than only detect the contingency itself. Furthermore, the advantage of 'soft decision' for the next generation of RAS has been discussed in [8]. Soft decision requires fast and adaptively detecting the system instability based on both events and responses from wide area monitoring. It has become possible with the deployment of real-time phasor measurements, as well as with modern communication ability.

1.2.3 Instability Phenomena and RAS

RAS is installed to preserve the integrity of network when instability phenomenon occurs in the power system. Since the RAS is often dedicated to a specific MOD, it is important to know which instability phenomenon the RAS is designed to prevent. Generally, system instability can be classified as transient instability, small signal instability and voltage instability. References [9-10] provide detailed description of these phenomena. Reference [6] further summarized the instability phenomena related to RAS design. They are:

- Transient instability

Transient stability is the ability of a power system to maintain synchronism when subjected to a severe disturbance such as a fault on transmission facilities, loss of generation or large load. The system response to such disturbances involves large excursion of generator rotor angles, power flow, bus voltages and other system variables. The transient instability can affect a single generating unit, a power plant, and one or more interconnected regions of network. The loss of synchronism may occur in the first swing or after a series of divergent swings.

- Small signal instability

Small signal stability is the ability of a power system to maintain synchronism when subjected to small disturbances. Small signal instability normally is caused by insufficient damping of oscillations in the system.

- Frequency instability.

Frequency stability is the ability of a power system to maintain the system frequency within an acceptable range during normal operating conditions or after a severe disturbance. Typically, power plants with underfrequency or overfrequency will be tripped when the deviation of the system frequency reaches a predetermined threshold, e.g., 2 Hz. Control actions need to be initiated before this threshold is hit.

- Voltage instability

Voltage stability is the ability of a power system to maintain acceptable voltage at all busses in the system under normal conditions and after a disturbance. Voltage instability is caused by insufficient reactive power support in some locations in the system. It usually takes the form of a progressive drop in voltage.

- Cascaded line tripping

Cascaded line tripping refers to an uncontrolled sequence of transmission line disconnections triggered by an incident at a single location. Generally, there are two common reasons for cascaded line tripping. One is the oscillations in real and reactive power flows and voltage instability. It may initiate some protective devices or control equipments, which can occasionally result in uncontrolled cascaded line tripping. The other is the overload or thermal problems of equipments.

Table 1.1 Most common RAS actions to counteract system instability phenomena

Control action	Transient instability	Small signal instability	Frequency instability	Voltage instability	Cascade line tripping
Generation rejection	+	+	+	+	+
Remote load shedding	+	+			+
HVDC fast power change	+	+	+	+	+
Braking resistor	+	+			
Controlled opening of ties	+	+	+	+	
Underfrequency load shedding			+		
Turbine fast valving	+	+	+		
Automatic shunt switching	+	+		+	
Undervoltage load shedding				+	
Tap changer blocking			+	+	
Actions on the AGC		+		+	+
Gas turbine start-up			+	+	+

Remedial action schemes that can be used to counteract these instability phenomena have also been listed in [6]. It is summarized as in Table 1.1.

Note that different power systems or different countries may have different classifications of RAS. The above classifications are from the CIGRÉ report, which are adopted by many European countries. According to the NERC Reliability Standards [11], Under Voltage Load Shedding (UVLS) and Under Frequency Load Shedding (UFLS) do not belong to RAS/SPS. There are some actions not listed in the above table but have been used in practice or been researched, for example:

- For voltage instability: control of series compensation; change of the generator voltage set point; reducing voltage set point at load center.
- For small signal instability: traditional PSS and the potential application of PSS with input from wide-area measurements [12].
- For frequency instability: changing the operating mode of a pump storage unit from pump load to generator, or reverse.

In addition, hydro or pumping storage unit start-up can also be used when there is a risk of voltage collapse caused by inadequate generation.

1.2.4 Practical Issues

Several common problems need to be resolved in RAS design. They are:

- How to detect the abnormal operating conditions?
- Where the RAS action will be taken?
- When the RAS action will be initiated?
- How much is the RAS MW or MVar requirement?

RAS design is a task of system planning in the current power industry practice. In the deregulated environment, the implementation of RAS is considered as an alternative to transmission expansion. Reliability and economic comparison are studied between the additional RAS and network expansion [13].

To select the locations of generation rejection and remote load shedding, several factors need to be considered in RAS design; for example, ma*RKE*t contract for generation and load; if RAS reject generation and/or load in firm contracts, the cost will

be very high. Following the RAS action, the operation guides normally require the system to recover in a limited amount of time. Generally, most thermal and nuclear generators cannot return to synchronism fast enough after dropping. Some hydro plants also cannot recover quickly because of the water conditions in the reservoir or along the river. Therefore, it is necessary to select the type and location of generation carefully for RAS in order to allow the system to recover within the required time.

There are also some requirements for the maximum allowable MW amount to be tripped in power systems. For example as indicated in [14], the maximum net generation rejection cannot exceed the maximum amount of the spinning reserves of the system, which is generally equal to the capacity of the maximum single unit. Is also required that the RAS input need to be as simple as possible. Normally, the input cannot be more than four signals [14].

1.3 Motivation and Contribution

1.3.1 Motivation

Although it does not often occur in the power system, the transient instability is still a severe threat to the power system security. Event-based open-loop control is normally utilized to implement the RAS for transient instability, and the generation rejection and remote load shedding are primarily selected as control actions. An example of the control logic that is utilized in practice is:

i) Monitor the transfer power on a specific transmission path. If the transfer power is greater than a pre-defined threshold, then arm the RAS.

ii) If a pre-defined event is detected such as, two lines tripping on a same tower simultaneously or within a short time window, then the RAS will be initiated.

The requirements on RAS, in current practice, tend to be obtained through repeated off-line simulations, which is so time consuming that many utilities can only update the RAS setting once every several years. Incorrect RAS setting may put the power system under serious risks such as, insufficient RAS rejection or even malfunction of RAS. Furthermore, the existing RAS are normally designed to trip generation enough for the worst scenario. For those scenarios that are less severe, the RAS may trip more generation and/or load than the actual need. Many utilities and ISO (Independent System Operators) have considered installing the stability assessment tools on-line to calculate the RAS requirements. Under the deregulation of the power system, fast calculation method of RAS and adaptive RAS design becomes more and more desirable and necessary.

The occurrence of the new technologies also encourages the research of the adaptive RAS. In recent years, utilities have started to install Phasor Measurement Units (PMU) in the power system. The synchronized measurements from PMU can provide the real time condition of the power system right following a disturbance. The PMU data can be used for instability prediction and wide area control. For those relative slow phenomena such as, voltage decay and inter-area oscillation with negative damping, it is possible to use the on-line feedback control to increase the system stability. For transient instability, although feedback control may not satisfy the time requirement on RAS, the PMU data can be used to detect the instability and trigger the open-loop RAS action. The amount of

the generation tripping or load shedding can also be determined based on the real-time system condition measured by the PMU.

To satisfy the requirements of the adaptive RAS, the off-line calculation needs to provide more information than only the MW value tripped for the worst scenario. Many other factors need to be considered in the calculation so that the results can consist of sufficient information for an on-line decision. The information may include the effect of the time delay and the fault location, and the system states following the disturbance, etc. Including new information into the off-line calculation also implies a heavier computational burden. Although the traditional repeated time domain simulation is still the workhorse for the RAS design, it is insufficient to accomplish these new tasks, because of not only the speed of the computation, but also the limited functionalities. Thus, it is would be valuable to develop the new calculation methods for an adaptive RAS.

The structure of the proposed RAS can be illustrated as Figure 1.2. Comparing to the Figure 1.1, a new block of instability detection is added before the block of the decision process. This new block will include the functionality that flexibly detects system instability based on the system response. The decision process is also different than in Figure 1.1. It is an adaptive process that can use the system response, such as the synchronized phasor angles, to make the decision. This new structure for the RAS will be built based on a new calculation methodology that will incorporate information of the system responses and will enable the adaptive on-line decision.

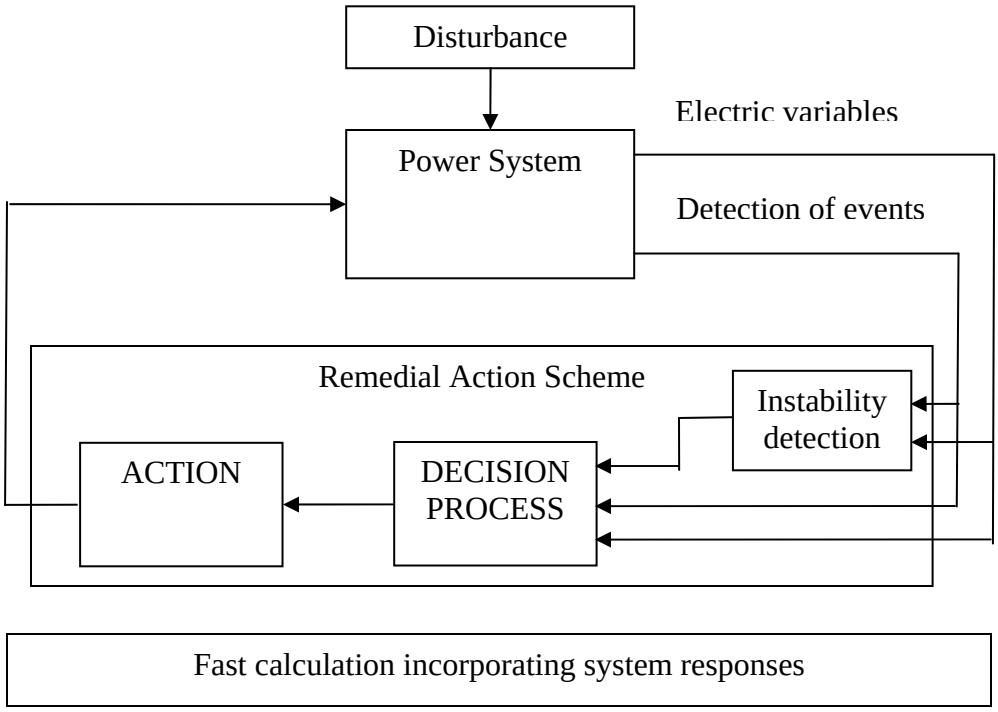

Figure 1.2 Modified structure of RAS

1.3.2 Contribution

An adaptive calculation method for RAS based on the transient energy criterion is proposed in this dissertation for the first time. Given a two-area system model and a MOD that the system will separate after a severe fault on the ties, the presented method separately calculates *DPE* and *RKE* with respect to an intermediary case. A sufficient RAS is determined by comparing the *RKE* and the *DPE*. Because the *DPE* can be reused for the new unstable cases, the repeated time domain simulation can be avoided in RAS calculation. This method is adaptive to different operating points and fault locations; it also can change with different fault clearing times and/or RAS initiation time. This method presents a way to reduce the time domain simulations in the RAS off-line

calculation. This method also enables us to establish an adaptive RAS using fast on-line computation.

A new approximate transient energy calculation method is proposed based on the curve of equivalent power versus equivalent angle (EPEA curve) of the power system, which is derived from the concept of corrected kinetic energy. It is particularly suitable for transient energy calculation in situations with varying mechanical power, such as generation rejection. This method can be used not only for generation transient energy calculation; but also to support the *DPE* calculation.

A concept using transient instability detection as the trigger of an adaptive RAS is also proposed. A decision tree technique is applied to detect system transient instability with PMU measurements as input. The decision trees include MOD information so that it is specific to the disturbance. This dissertation investigates the impact of PMU time delay, synchronization, placement and precision, and so on; as well as the impact from other input features such as system events and pre-disturbance operating conditions. Transient instability detection based on the presented design of the decision trees shows promise for high robustness and accuracy, based on the presented numerical examples.

1.3.3 Scope of this work

This dissertation will mainly focus on key aspects of the adaptive RAS for the transient instability, particularly, a new calculation method for generation rejection and load shedding. The adaptive calculation method of RAS is based on the transient energy criterion. The EPEA curve is used to support the transient energy calculation in the RAS. The practical issues in the RAS calculation such as, RAS location and time delay will be analyzed. Robustness of the proposed method will be evaluated. Since the transient

energy method is utilized, only first-swing unstable cases are studied. IEEE 39-bus system and the WECC 179-bus simplified system are used to test the effectiveness and the robustness of the proposed methods.

The real-time transient instability detection based on decision trees and phasor measurements are studied. The decision trees are designed to include the information of MOD so that they can be used as the trigger of RAS for a specific MOD. By using an open source software package, C4.5 [15], to construct the decision trees, the main efforts will be given to investigating the practical issues that will affect the performance of the detection. The investigated issues include:

- Time delay associated with PMU measuring and communication, including measurement availability associated with the timing issues.
- The synchronization of PMU sampling as independent of the occurrence of system events.
- The placement of PMU at generator busses and other busses.
- Various input features.

1.4 Literature review

1.4.1 Literature review for RAS calculation

The CIGRÉ report [6] summarized the RAS practices in the power industry till 2001. According to this report, the requirements of RAS can be identified as the necessary actions to satisfy the system performance criteria; this tends to be found by an iterative procedure between the instability determination and RAS action simulation for the given

severe contingencies. The instability is determined by any of several methods but most commonly by extensive time domain simulations since computations are off-line. Still, several other methods can be employed to accelerate the computation such as, the transient energy method [16-19], the coherency index method [5] and the EEAC or SIME [20-21]. After screening for the severe contingencies, a database or lookup table can be established for on-line decision [19-20]. Data mining techniques can also be employed to establish on-line operation rules for RAS [22]. The determination of a RAS can also be combined with the computation of preventive control to provide comprehensive control for a pre-defined system disturbance [21].

There are two common assumptions for most of these studies. First, they assume the control action does not change the MOD [17]. Second, the control schemes are established based on predefined scenarios, i.e., a control action is determined given an operating point and fault scenario. For those scenarios that are not predefined the closest neighborhood method can be used, but it may be inaccurate in practice. Furthermore for the RAS to find a sufficient action, engineers need to repeat numerical simulation on many candidate actions. Although these computations are off-line, frequent update for new operation conditions is still necessary and the computational burden and testing are key issues for implementation. An adaptive method for RAS is presented in [23-25], which become a part of this dissertation. The detail of the adaptive RAS will be discussed in Chapter 2 through Chapter 4 of this dissertation.

1.4.2 Literature review for real-time transient instability detection

Transient stability assessment has been studied for many years. Many efforts have been made on the fast calculation of the system response and the stability index in real

time. There are several well-known methods such as transient energy method [16, 18], EEAC or SIME [26-27], and the coherency index method [5]. These methods are adaptive to the variation in the operating conditions, such as operating points, topology of the network and fault scenarios. However, under the limitation of computational techniques, both in software and hardware, these methods still cannot satisfy the requirements of real-time transient stability assessment. On the other hand, intelligent system (IS) type methods, such as decision trees and neural networks, can be trained off-line and applied on-line. Following a contingency, a well-trained decision tree or neural network can assess whether the system is stable or unstable based on the pattern recognition for the current operating condition. Reference [28] comprehensively introduces the IS methods and their application on the stability assessment of power system, where the assessment is mainly based on the pre-fault operating points and fault scenarios (location and clearing time).

The measurements of a PMU are synchronized based on the Global Positioning System (GPS) so that the measured phasor angles from dispersed locations in a power system can be compared on the common time reference axis [29] both in the steady-state and following disturbances. Some efforts have been directed at the use of real-time PMU measurements for on-line stability prediction. An adaptive out-of-step relay is proposed in [30] by using the measured angles at busses on both sides of the tie lines. A curve-fitting method is used in [31] where rotor angles of generators are predicted by extrapolating the measured angles in a short time window. The curve-fitting method may not work well sometimes because of the complexity and nonlinearity of the power system. Alternatively, decision trees for real time transient instability prediction based on

the phasor measurements are investigated systematically in [32]. Several issues with respect to the PMU measurements have also been discussed in the same paper such as, the precision and synchronization in the phasor measurements and the robustness of the decision trees. In [33] voltage angles measured by PMU are used as input of decision trees to predict the voltage insecurity.

Real-time transient instability detection based on decision trees and phasor measurements is designed as the trigger of the RAS action in [34], which is discussed in Chapter 5 of this dissertation. The practical issues that will affect the performance of the decision trees are studied in detail on IEEE 39-bus system and WECC 179-bus system.

Chapter 2

TRANSIENT STABILITY AND TRANSIENT ENERGY METHODS

2.1 Fundamental of transient energy method

As described in Chapter 1, transient stability is the ability of a power system to maintain synchronism when subjected to a severe disturbance such as a fault on transmission facilities, loss of generation or large load. The system response to such disturbances involves large excursion of generator rotor angles, power flow, bus voltages and other system variables.

The power system can be modeled by the differential-algebraic equations (DAE):

$$\begin{aligned} \dot{x} &= f(x, y) \\ 0 &= g(x, y) \end{aligned} \tag{2.1}$$

where x is the vector of state variables that includes the rotor angle and speed of generators, and other state variables of control devices such as, exciter, PSS and governor. In (2.1), $0=g(x, y)$ is the power flow equations and y is the vector of algebraic variables consisting of voltage angle and magnitude of busses of the power system.

The system stability can be assessed by observing the separation among rotor angles of generators in a time-domain simulation, which is to solve (2.1) by an explicit or

implicit integration method. Time domain simulation has been extensively utilized in transient stability analysis because of its flexibility in system modeling; however, it does not provide a quantitative stability index, i.e., how far the system is from the boundary between the stability and instability and this is the main disadvantage of time domain simulation.

Alternatively, the transient energy method provides a quantitative stability index by calculating the Lyapunov energy of the non-linear power system [16]. Among the differential equations, the equations for rotor angle and speed in the Center of Angles (COA) frame are:

$$M_i \frac{d\omega_i}{dt} = P_i - P_{ei} - \frac{M_i}{M_T} P_{COA}, i = 1, \cdots, N \tag{2.2}$$

$$\frac{d\theta_i}{dt} = \omega_i, i = 1, \cdots, N \tag{2.3}$$

where, M_i is the inertia constant for generator i and $M_T = \sum_{i=1}^{N} M_i$. $\theta_i = \delta_i - \delta_0$ is the rotor angle in the COA frame with $\delta_0 = \frac{1}{M_T} \sum_{i=1}^{n} M_i \delta_i$, while δ_i is the angle in the synchronous frame. Similarly, the rotor speed ω_i in the COA frame is defined by $\omega_i = \varpi_i - \varpi_0 = \dot{\delta}_i - \dot{\delta}_0$. The acceleration power is $P_{COA} = \sum_{i=1}^{N} (P_{mi} - P_{ei})$. Note, the angle and speed in COA frame have the property $\sum_{i=1}^{N} M_i \theta_i = \sum_{i=1}^{N} M_i \omega_i = 0$.

The transient energy defined for the post-fault system is:

$$V = V_{KE} + V_{PE} \tag{2.4}$$

where

$$V_{KE} = \frac{1}{2}\sum_{i=1}^{N} M_i \omega_i^2 \tag{2.5}$$

$$V_{PE} = -\sum_{i=1}^{N} \int_{\theta_i^S}^{\theta_i} P_{acc\,i}(\theta) d\theta \tag{2.6}$$

$$P_{acci}(\theta) = P_{mi} - P_{ei} - \frac{M_i}{M_T} P_{COA} \tag{2.7}$$

Following a severe contingency, the generators in the system may separate into two groups: the critical machines, which tend to separate from the system, and the rest of the generators. The centers of angle of these two groups have inertia constants and angular speed M_{cr}, ω_{cr} and M_{sys}, ω_{sys} respectively. The corrected kinetic energy, which is the portion of the kinetic energy contributing to system separation, is given in [16]:

$$V_{KEcorr} = \frac{1}{2} M_{eq} \omega_{eq}^2 \tag{2.8}$$

where $M_{eq} = \frac{M_{cr} M_{sys}}{M_{cr} + M_{sys}}$, $\omega_{eq} = (\omega_{cr} - \omega_{sys})$, $M_{cr} = \sum_{i=1}^{N_c} M_i$, $M_{sys} = \sum_{i=1}^{N_{sys}} M_i$,

$\omega_{cr} = \frac{\sum_{i=1}^{N_c} M_i \omega_i}{M_{cr}}$, $\omega_{sys} = \frac{\sum_{i=1}^{Nsys} M_i \omega_i}{M_{sys}}$, N_c is the number of critical machines, and N_{sys} is the number of remaining machines. Therefore, the corrected kinetic energy is the kinetic energy of the critical machines relative to the remaining system. It is the same as the kinetic energy of an equivalent one machine infinite bus (OMIB) system having inertia constant M_{eq} and angular speed ω_{eq} [16].

Stability is assessed by checking the sign of the energy margin:

$$\Delta V = V_{cr} - V_{cl} \tag{2.9}$$

where V_{cr} is the critical energy at Controlling Unstable Equilibrium Point (CUEP) and V_{cl} is the energy at the clearing point. The CUEP is determined by the MOD, i.e., how will the system separate into critical and remaining groups after a severe disturbance. Then, the criterion for transient stability is:

- If $\Delta V > 0$ then system is stable.
- If $\Delta V < 0$ then system is unstable.

A key issue of transient energy method is to find the CUEP. Many efforts have been made by researchers to improve the accuracy in searching for the CUEP. Outstanding works include [16, 18, 35-40].

2.2 Hybrid method for transient energy calculation

Compared with the time domain simulation, the transient energy method faces a limitation in handling complicated system models. Several methods have been proposed to combine the advantages of both time domain simulation and transient energy method. This is so-called hybrid method [18, 39-40]. The point where the system trajectory crosses the Potential Energy Boundary Surface (PEBS) is used to approximate the CUEP in the hybrid methods. The residual kinetic energy at the PEBS crossing point is used as the energy margin of an unstable case. For a stable case, the kinetic energy will return to zero before the trajectory reaches the PEBS. The energy margin is estimated by the

potential energy between the PEBS and the point where the kinetic energy is zero. This computation is realized by adding one [18, 39] or a series [40] of pseudo faults at the time when the kinetic energy is zero. The pseudo faults are selected to cause the system to be critical unstable. The energy margin is the difference between the injected kinetic energy and the residual kinetic energy at the PEBS crossing point plus a compensation for the position change along the trajectory caused by the pseudo faults. The hybrid methods proposed in [18, 39], where only a single pseudo fault is used, is specifically named the Second Kick method.

The EEAC [26] or SIME [27] methods project the system to the angle space and further found an equivalent OMIB system; hence, the transient energy can be calculated by the areas of acceleration and deceleration. PEBS also plays an important role in EEAC and SIME, although not explicitly, since the equivalent OMIB can only be obtained on the angle space. EEAC or SIME also belong to the class of hybrid methods.

As explained in [16], the PEBS is the stability boundary of the associated gradient system, which is described by:

$$\dot{\theta}_i = -\frac{\partial V_{PE}(\theta)}{\partial \theta_i},\ i = 1, \cdots, N \tag{2.10}$$

where $V_{PE}(\theta)$ is given by (2.6)

Although [37] has proved that PEBS might not give a conservative approximation of CUEP in some situations, the hybrid methods have wo*RKE*d well in practical power systems and provided fast assessment of transient instability.

Besides the above hybrid methods that combine the time domain simulation and transient energy method, others have made an effort from a different direction where the

coherency index was derived from rotor angles and/or speed, or their combinations [5]. This index then is used to assess the system stability. This method can provide a quantitative index for the system stability and use the sensitivity of the coherency index to reschedule the generation as a preventive control. Similar to the coherency index sensitivity, the trajectory sensitivity method is also applied to system stability analysis in [41], but it is mainly used for small disturbance since it requires the linearization in the small neighborhood around the original operating points.

2.3 Transient energy calculation based on the EPEA curve

Focusing on efficiently calculating the MW requirement of a RAS action, a new transient energy calculation method is proposed based on the curve of the equivalent power versus the equivalent angle (EPEA curve). It belongs to the hybrid method, but is particularly appropriate for the RAS calculations.

2.3.1 Equivalent power and equivalent angle

Adding together the differential equations (2.2) of critical generators and dividing both sides of the equation by M_{cr}, we have:

$$\frac{1}{M_{cr}}\sum_{i=1}^{N_{cr}} M_i \dot{\omega}_i = \frac{1}{M_{cr}}\sum_{i=1}^{N_{cr}} (P_i - P_{ei}) - \frac{1}{M_T} P_{COA} \tag{2.11}$$

Similarly, for the generators of the remaining group we have:

$$\frac{1}{M_{sys}}\sum_{i=1}^{N_{sys}} M_i \dot{\omega}_i = \frac{1}{M_{sys}}\sum_{i=1}^{N_{sys}} (P_i - P_{ei}) - \frac{1}{M_T} P_{COA} \tag{2.12}$$

Subtracting (2.2) from (2.11) and multiplying by M_{eq} gives:

$$M_{eq}\dot{\omega}_{eq} = \frac{M_{sys}}{M_T}\sum_{i=1}^{N_{cr}}(P_i - P_{ei}) - \frac{M_{cr}}{M_T}\sum_{i=1}^{N_{sys}}(P_i - P_{ei}) \tag{2.13}$$

Then, multiplying by ω_{eq} and integrating with respect to t, we obtain:

$$\frac{1}{2}M_{eq}\omega_{eq}^2 = \int_{t0}^{t}\left[\frac{M_{sys}}{M_T}\sum_{i=1}^{N_{cr}}(P_i - P_{ei}) - \frac{M_{cr}}{M_T}\sum_{i=1}^{N_{sys}}(P_i - P_{ei})\right]\omega_{eq}dt \tag{2.14}$$

Now define the equivalent angle between two groups as:

$$\theta_{eq} = \theta_{cr} - \theta_{sys} \tag{2.15}$$

where $\theta_{cr} = \frac{\sum_{i=1}^{N_c} M_i\theta_i}{M_{cr}}, \theta_{sys} = \frac{\sum_{i=1}^{Nsys} M_i\theta_i}{M_{sys}}$. The equivalent angle is simply the angle difference between the centers of angle of two groups in the power system.

Then, by substituting the equivalent angle for the time as the integral variable in (2.14), we can obtain:

$$\frac{1}{2}M_{eq}\omega_{eq}^2 = \int_{\theta_{eq}^s}^{\theta_{eq}}\left[\frac{M_{sys}}{M_T}\sum_{i=1}^{N_{cr}}(P_i - P_{ei}) - \frac{M_{cr}}{M_T}\sum_{i=1}^{N_{sys}}(P_i - P_{ei})\right]d\theta \tag{2.16}$$

where θ_{eq}^s corresponds to the stable equilibrium point respectively. In (2.16), the left side is the corrected kinetic energy as in (2.8), and the right side is the system potential energy described by integration with respect to the equivalent angle. We define the integral function of (2.16) as the equivalent power between two groups:

$$P_{eq} = \frac{M_{sys}}{M_T}\sum_{i=1}^{N_{cr}}(P_i - P_{ei}) - \frac{M_{cr}}{M_T}\sum_{i=1}^{N_{sys}}(P_i - P_{ei}) \tag{2.17}$$

Similar derivations can be found in [39]. The corrected kinetic energy is the same as that of an equivalent OMIB system having inertia constant M_{eq} and angular speed ω_{eq}, as pointed out in [16]. Then the right side of (2.16) defines the potential energy of the equivalent OMIB system. Considering the equivalent power as a function of the equivalent angle, a curve of P_{eq} versus θ_{eq} can be plotted. It is known that the P_{eq} is the acceleration power of the equivalent OMIB system, i.e., when the equivalent power is positive the critical group accelerates with respect to the rest of the system, otherwise it decelerates. The area enclosed by the curve of P_{eq} versus θ_{eq} and the horizontal axis (P_{eq}= 0) reflects the transient energy of the power system. Comparing with EEAC or SIME, the equivalent power is not further split into mechanical and electrical power. The equilibriums of the equivalent OMIB system always occur on the horizontal axis. The changes of the mechanical power, caused by generation rejections or governors, will be reflected on the curve. As in other hybrid methods, the full system dynamic model can be used in the transient energy calculation based on EPEA curve. Note that using the EPEA curve to express the transient procedure of the power system is equivalent to reducing the system from the (θ, ω) space to the (θ) space. This implies that the PEBS is used to approximate the stability boundary.

2.3.2 Calculating the transient energy and energy margin – Unstable case

The examples used in this and the next subsections are the same IEEE 39-bus system that will also be used for illustrating the RAS calculation in Chapter 4. The system description can be found in Chapter 4.

Figure 2.1 shows the EPEA curve of an unstable case. The positive part of the area enclosed by the curve and the horizontal axis is the acceleration area while the negative part of the enclosed area is the deceleration area. The acceleration area A_{acc} and deceleration areas A_{dec} are calculated by:

$$A_{acc} = \int_{\theta=a1}^{\theta=a2} P_{eq}\left(\theta_{eq}\right) d\theta \tag{2.18}$$

$$A_{dec} = \int_{\theta=a2}^{\theta=a3} P_{eq}\left(\theta_{eq}\right) d\theta \tag{2.19}$$

At the point a2 and a3 in Figure 2.1, the equivalent power is zero. They correspond to the stable and unstable equilibrium points, respectively, of the equivalent OMIB system. Figure 2.2 is the curve of the corrected kinetic energy for the same example. If the minimum kinetic energy is greater than zero, then the PEBS crossing occurs and it indicates the system is unstable. Thus, the negative of this minimum kinetic energy can be used as the energy margin for the unstable case [18]. In the OMIB system, this point is corresponds to the unstable equilibrium point, i.e., the point a3 in Figure 2.1. The energy margin for the unstable case can also be obtained by:

$$EM = A_{dec} - A_{acc} \tag{2.20}$$

From the OMIB system, it is also known that the maximum kinetic energy after the fault clearing is equal to the acceleration area. It is true for both unstable and stable cases.

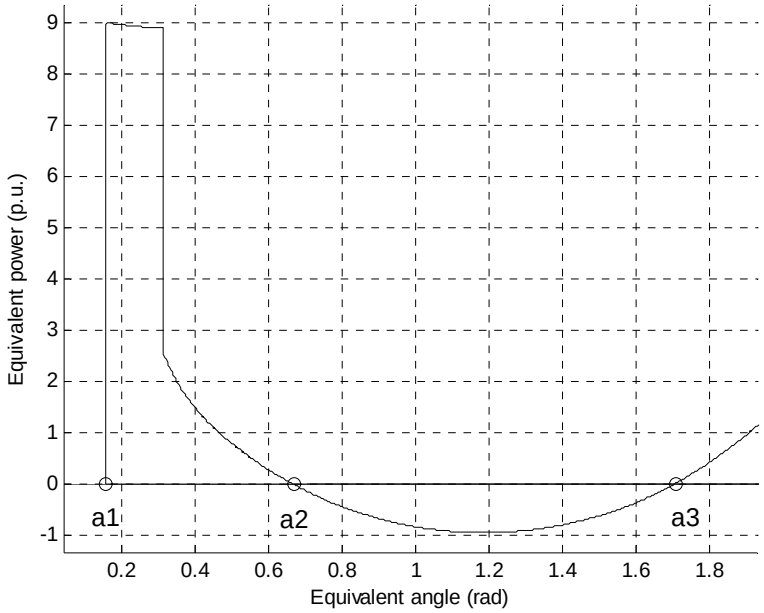

Figure 2.1 Unstable case – EPEA curve

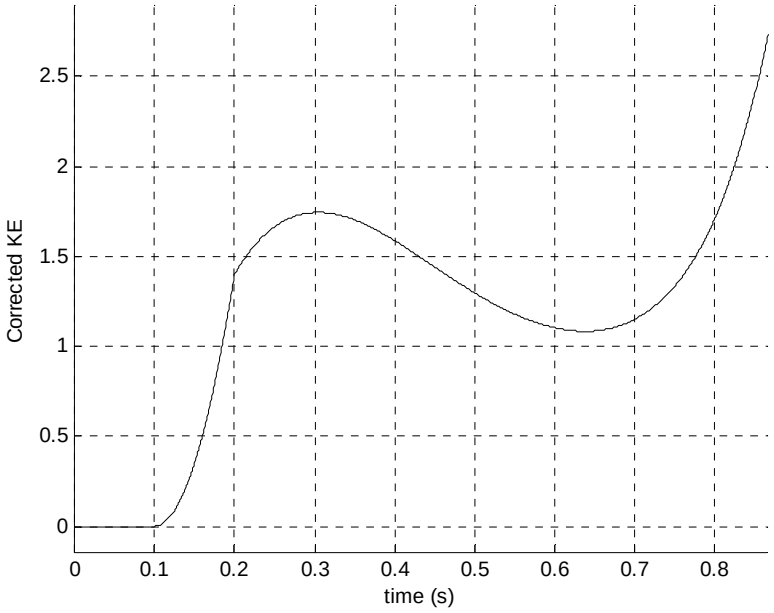

Figure 2.2 Unstable case – Corrected kinetic energy

Table 2.1 Key values on the curves of Figure 2.1 and Figure 2.2

Max. KE	Min. KE	A_{acc}	A_{dec}	A_{dec}-A_{acc}	P_{eq} for Max KE	P_{eq} for Min KE
1.7440	1.0833	1.7441	0.6608	-1.0833	-0.0096	-0.0101

The comparison between Figure 2.1 and 2.2 is summarized in Table 2.1. It can be seen that the acceleration area is equal to the maximum KE before the system becomes unstable; the minimum KE is equal to the difference between the acceleration and the deceleration areas. The P_{eq} at the points with maximum KE and minimum KE are close to zero, i.e., they are the equilibrium points.

Note that the above study case does not include the governors in the dynamic model. The proposed method can also be applied for cases with governors in service. That means using the EPEA curve can calculate the transient energy for the cases with varying mechanical power. Figure 2.3 shows the EPEA curve of an unstable case with governors in service. Figure 2.4 is the corresponding corrected KE.

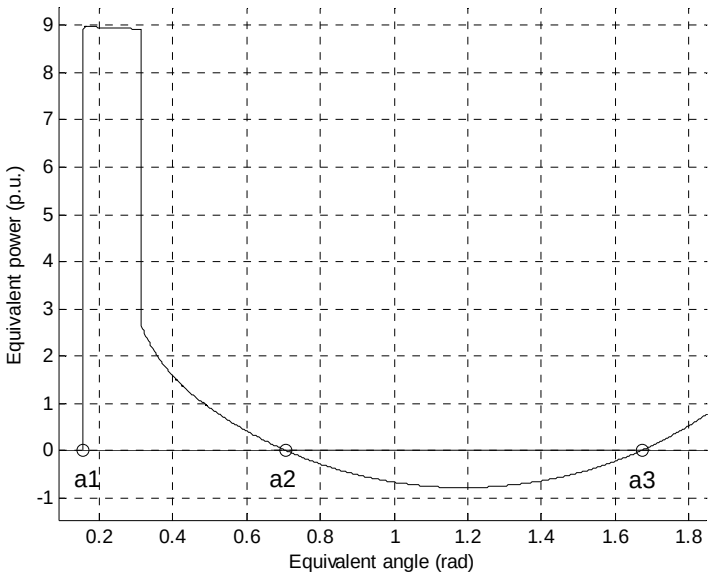

Figure 2.3 Unstable case with governors – EPEA curve

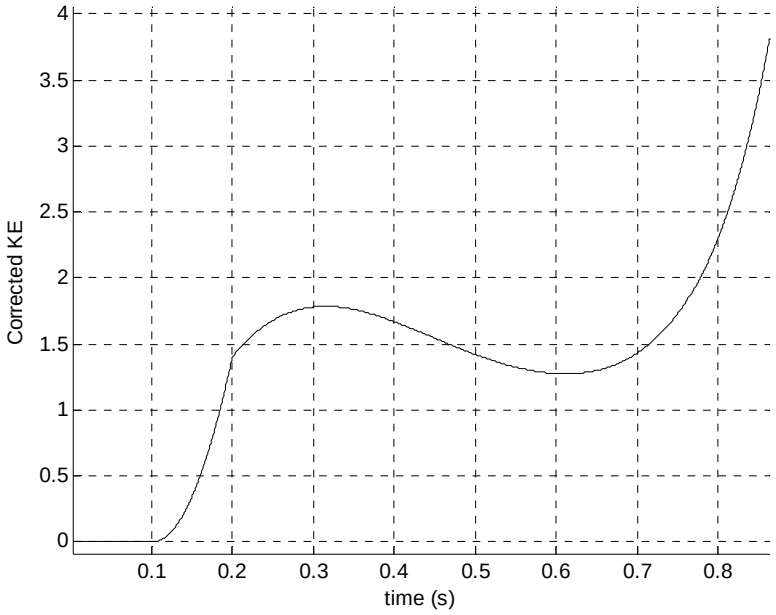

Figure 2.4 Unstable case with governors – Corrected kinetic energy

Table 2.2 Key values on the curves of Figure 2.3 and Figure 2.4

Max. KE	Min. KE	A_{acc}	A_{dec}	A_{dec}-A_{acc}	P_{eq} for Max KE	P_{eq} for Min KE
1.7859	1.2739	1.7860	0.5120	-1.2740	0.0007	0.0017

Similar to Table 2.1, the comparison between Figure 2.3 and Figure 2.4 are summarized in Table 2.2.

The governor can continuously adjust the mechanical power of the generator, so that the EPEA curve in Figure 2.3 is a smooth curve. Generator rejection initiated by a RAS will cause a sudden change on the mechanical power, then the EPEA curve will have a discontinuity; still, the EPEA curve can be used to calculate the transient energy when there is generation tripping. This will be illustrated in Chapter 3.

The EPEA curve is different from EEAC [26] or SIME [27], which use two curves, the equivalent electrical power and the equivalent mechanical power, to express the equivalent OMIB system. Two different curve fittings are needed in EEAC or SIME when the mechanical power varies, which increases the complexity and the accuracy of the calculations may be reduced.

2.3.2 Calculate the transient energy and energy margin – Stable case

For a stable case, which is illustrated in Figure 2.5 and Figure 2.6, there is not an enclosed deceleration area between the curve and the horizontal axis. The deceleration area, i.e. the potential energy, can be calculated from:

$$A^{dec} = KE_{orig}^{\max} + EM \tag{2.21}$$

where $KE_{orig}^{\max}$ is the maximum kinetic energy injected by the original fault. EM is the energy margin of the system.

Second Kick method can be used to find the energy margin:

$$EM = KE_{sk}^{\max} - KE_{sk}^{\min} + PE_{sk}^{comp} \tag{2.22}$$

where $KE_{sk}^{\max}$ is the maximum kinetic energy injected by the second kick; $KE_{sk}^{\min}$ is the minimum kinetic energy after clearing the second kick; and PE_{sk}^{comp} is the compensation for the potential energy change caused by the second kick. Details of the Second Kick method can be found in [18]. Different from [18], the PE_{sk}^{comp} will be calculated on the EPEA curve in this dissertation.

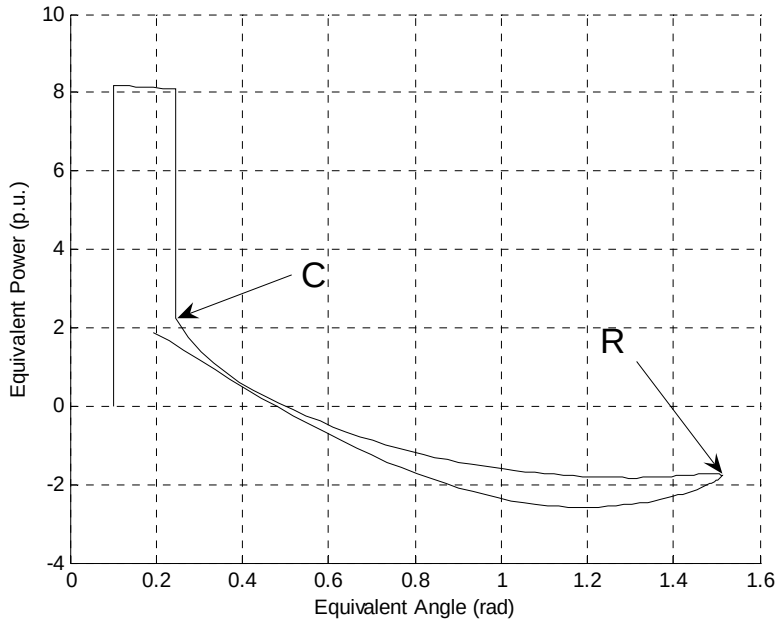

Figure 2.5 Stable case – EPEA curve

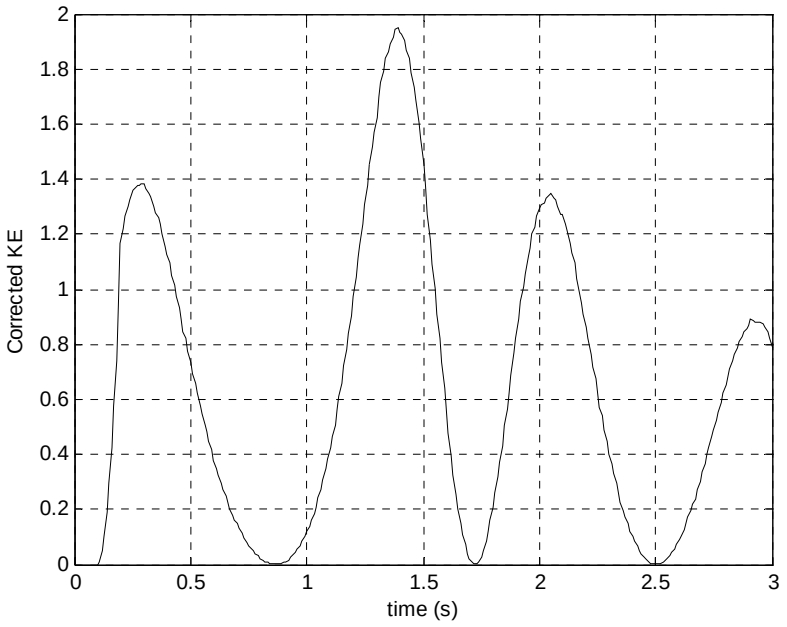

Figure 2.6 Stable case – Corrected kinetic energy

We can also use a curve-fitting method that assumes the equivalent power is a triangular function of the equivalent angle. This reduces the off-line computations by eliminating the need for the pseudo fault in the Second Kick Method. Let:

$$P_{eq-fit} = \alpha + \beta \cos(\theta_{eq}) + \gamma \sin(\theta_{eq}) \tag{2.23}$$

For the curve-fitting method, we need to select sampling points in an extensive range from the fault clearing point to the point with the maximum equivalent angle, i.e., from point C to point R in Figure 2.5. Least-squares estimation will be used to calculate the parameters in (2.23). The energy margin is the area between the extrapolated part of the curve and the horizontal axis, and the calculation of the energy margin will be a simple integration. Figure 2.7 illustrates the Second Kick and curve-fitting methods on the EPEA curve for a stable case.

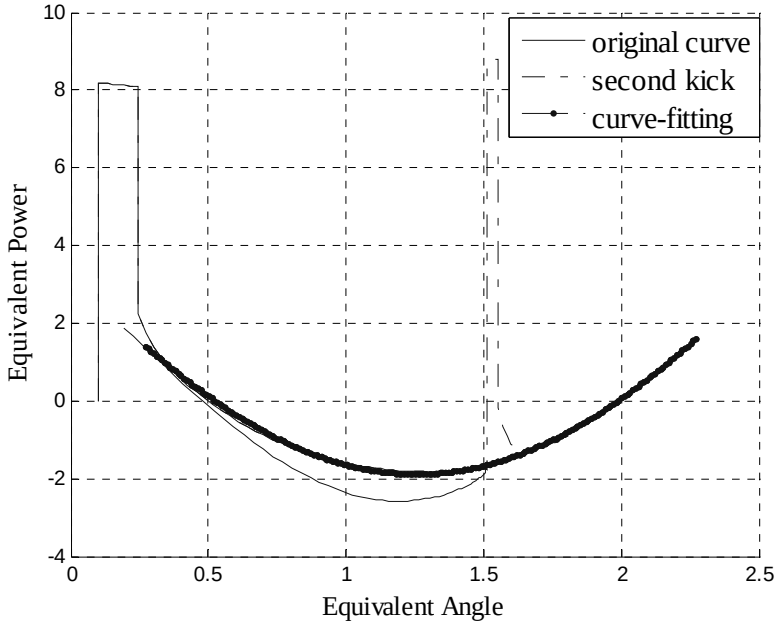

Figure 2.7 Second Kick and curve-fitting on EPEA curve

2.3.3 Energy margin versus transfer power

Similarly to [42], a nearly linear relationship between the energy margin and the transfer power can also be obtained by using the proposed EPEA method. It is illustrated in Figure 2.8, where the transfer power is expressed by the generation output of a generator. For the unstable cases, the energy margins are obtained from the minimum kinetic energy. For the stable cases, the energy margin can be obtained by either the Second Kick (in solid line) or curve-fitting method (in dash line). The stability limit can be approximated by the point where the energy margin is zero. In this example, it is expressed by the generation output of G_{35}, which is the generation on bus 35 in the IEEE 39-bus system. From Figure 2.8, the transfer limit corresponds to G_{35}=465MW, which is very close to the result from the repeated time domain simulations, 467MW. It can be seen that for this example, the Second Kick method gives a more conservative approximation for the energy margin of stable cases.

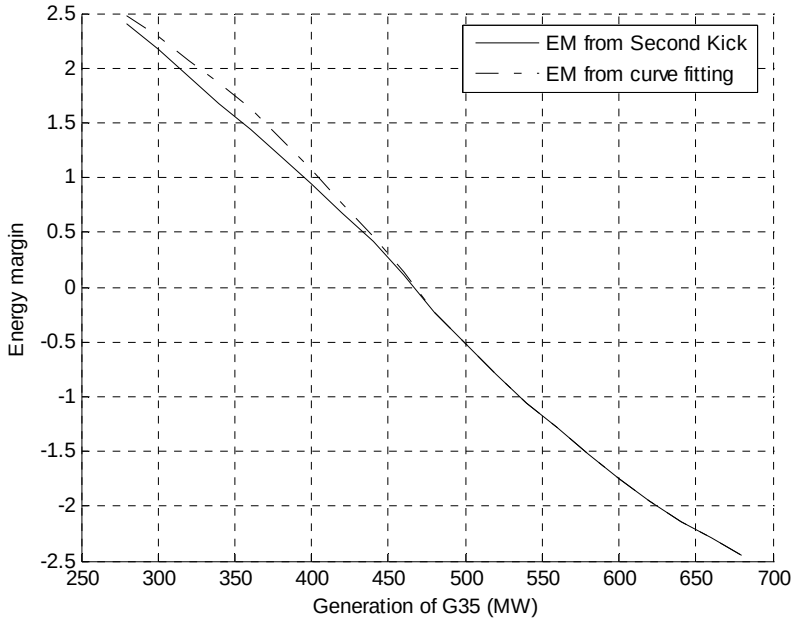

Figure 2.8 Energy margin vs. transfer power

Chapter 3

ADAPTIVE RAS COMPUTATION

3.1 Transient energy criterion for RAS computation

A RAS is designed to reduce the acceleration of the accelerated group of generators. To fulfill this purpose, the accelerated generators, hence the MOD, have to be determined first. When applying the transient energy method to the RAS computation, a crucial assumption is that the MOD will be unchanged by the control actions. This assumption is practical for first swing unstable cases, as pointed out in [6] and [17], and is supported by numerous time domain simulations during the author's research.

Following the analysis in [16], it is known that the CUEP is determined by the MOD. That means for a given post-fault network topology and dispatch pattern, if some different faults cause the same MOD, then the same CUEP is known. So, the critical energy is independent of these faults. An instance of this situation can be found in a two-area system model. For faults that occur along the tie lines at the different locations, the post-fault system has the same topology assuming the fault clearing action trips the faulted line.

Now suppose the RAS requires generation rejection and assume the RAS does not change the MOD. A similar concept can be applied to analyze the change of transient

energy during the transient procedure and following RAS actions. We define the following:

- An *analysis* case is the steady-state operating condition that requires a RAS to maintain stability after a severe contingency.
- A *reference* case will be the steady-state operating condition following some RAS action.

If the critical energy of a reference case is greater than the initial energy of the analysis case at the time the RAS is initiated, then the reference case will provide sufficient action. Then the amount of a RAS is the difference of generation between the analysis case and the reference case.

One could compare the energy of an analysis case with a set of candidate RAS reference cases to find an adequate scheme. Still, the assumption that the RAS action will not change the MOD tells us that for a given network topology and dispatch pattern, the critical energy of a reference case is fixed and independent of the analysis cases. This suggests that many of the computations in a repeated simulations approach to determining a RAS are not necessary.

To illustrate this further, consider Figure 3.1 where the PEBS is used to approximate the stability boundary of the system. Suppose there are two reference cases and one analysis case. The two reference cases are identified as critical, *cr*, and candidate, *ca*, cases, respectively. A RAS to reduce generation and load by the difference between the analysis case and case *cr*, i.e., case *cr* is the reference for the control action, still leads to instability since the system trajectory will cross the PEBS of case *cr*. On the other hand, using case *ca* as the reference for the RAS action stabilizes the system.

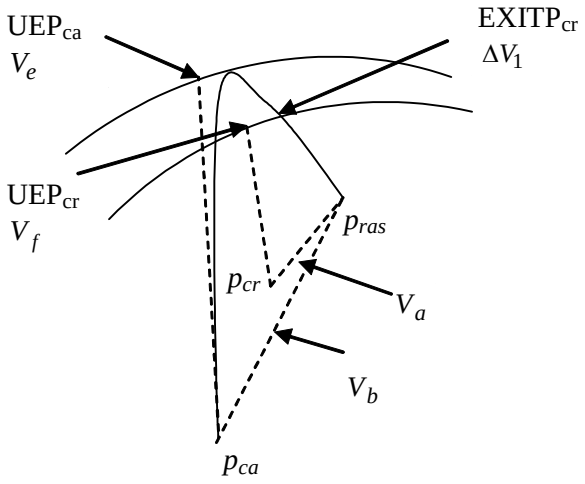

Figure 3.1 Energy comparisons of different cases

The points p_{cr} and p_{ca} are the Stable Equilibrium Point (SEP) of the reference cases, while UEP_{cr} and UEP_{ca} are the corresponding CUEPs. The potential energy at UEP_{cr} and UEP_{ca} is V_f and V_e, respectively. The point p_{ras} is a point on the trajectory of the analysis case when the RAS action is taken. At p_{ras}, the analysis case has kinetic energy V_0. If the RAS is determined by the critical case, there will be a residual kinetic energy ΔV_1 when the trajectory arrives at the stability boundary of the p_{cr}. Now suppose the potential energy at point p_{ras} corresponding to p_{cr} and p_{ca} are V_a and V_b, then the following equations hold:

$$V_a + V_0 = V_f + \Delta V_1 \tag{3.1}$$

$$V_b + V_0 = V_e \tag{3.2}$$

$$V_b = V_a + V_h \tag{3.3}$$

where V_h is the compensation for potential energy between the two reference cases. From (3.1)~(3.3), a new relationship among these three cases is found:

$$V_e = V_f + V_h + \Delta V_1 \tag{3.4}$$

After rearranging and allowing for an adequate stability margin, it can be used as a criterion for the needed RAS:

$$\Delta V_1 < V_e - V_f - V_h \tag{3.5}$$

By this criterion, the RAS computation is separated into two parts:

1) Using case *cr* as the reference of the RAS action and calculating the residual kinetic energy (*RKE*), which is ΔV_1 in (3.5);
2) Calculating the difference of potential energy (*DPE*) of case *cr* and some other reference case, e.g. case *ca*, which is the right hand side of (3.5).

The final RAS action is determined by requiring:

$$RKE < DPE \tag{3.6}$$

For a given system topology and operating point, if the MOD does not change following different faults or control actions, the potential energy V_f and V_e will not change. The compensation for potential energy V_h depends on the point p_{ras}, i.e., depends on the angles of generator at the time the RAS is taken, which causes *DPE* to be fault and RAS dependent. Using the approximated method of *DPE* given in the next sections, the *DPE* can be calculated without prior knowledge of the angles of generators at the point p_{ras} for a range of operating points.

3.2 Implementation of adaptive RAS computation

3.2.1 Two-area system model

Given the MOD assumption, a two-area system can be used to further simplify the RAS computation. A typical two-area system has the following characteristics:

- Given a topology and a fault scenario, there exists a transfer limit across the tie lines.
- When the transfer power is greater than the transfer limit, faults on ties and key transmission lines always cause the same MOD. The generators in the supply area will be accelerated with respect to those in the demand area.
- If the system is unstable after the disturbance, it may be insufficient to merely reduce the transfer power down to the transfer limit. For most cases, more generation and possibly load must be dropped in both areas. This means a scenario at the transfer limit does not provide an adequate estimate of the energy margin.
- The criterion of (3.6) can provide insight to the amount of needed generator dropping or load shedding.

For brevity, the two-area system model is used to illustrate the proposed method, so that the step to find a MOD is not needed. More methods for finding the MOD can be found in [16].

A three-step procedure can be used to determine the requirement of a RAS action for a given unstable case in a two-area system:

1) Simulate the rejection of generation in the supply area and load shedding in the demand area so that the transfer power is reduced to the transfer limit. Find the minimum kinetic energy after the control action, which is the *RKE*.
2) Calculate the *DPE* between the operating point achieving the transfer limit and those below the transfer limit. The *DPE* reflects the ability of the system to absorb excessive kinetic energy.
3) Reject generation and shed load in both areas to the operating point whose *DPE* calculated as in 2) satisfies $RKE < DPE$.

It has been analyzed in the previous section that the *DPE* can be reused to determine RAS action for the specific MOD. Therefore, only the first and third steps are needed in the RAS calculation for new unstable cases.

Generally, the *RKE* can be calculated with respect to any feasible operating point, identified as critical, *cr*. Then, the *DPE* are calculated with respect to the same critical operating point for the cases which have less transfer power than *cr* has. They are identified as candidate, *ca*. The operating point reaching the transfer limit is a convenient choice for the critical operating point, which can be obtained from any of a number of dynamic security assessment tools.

3.2.2 General computational procedure of adaptive RAS

Using the two-area system model and the computation criterion in the previous section, an adaptive RAS can be calculated for faults along the key transmission paths. The computation procedure is as following.

1) Select a critical reference case, which may be the case with the transfer limit, or with the operational transfer capability.

2) Find the *DPE* for each candidate case with respect to the critical case.
3) Use linear regression method (or other data fitting methods) to find a relationship between the *DPE* and the generation output.
4) Given an analysis case (with a given operating point and fault), calculate the *RKE* with respect to the critical case.
5) Repeat step 4 for different RAS analysis cases and apply a regression method to find a relationship between the *RKE* and fault locations as well as operating points.
6) From the relationship obtained in step 5 above find a value of *RKE* and compare with the corresponding *DPE* obtained in step 3 above.
7) Determine a qualifying reference case using the criterion (3.6): $RKE < DPE$.
8) A sufficient RAS action can then be determined by the difference between the RAS analysis case and the qualifying RAS reference case.

The above eight step procedure can be used in sequence for off-line RAS design. It can replace the conventional RAS design method to avoid unnecessary repeated simulations. The off-line study results will be used to establish a decision tool, such as look-up table, for on-line determination of the RAS action. Artificial Neuron Network (ANN), or other pattern matching approaches, can also be used to determine RAS action in real time. Because of the fast computation capability of the proposed RAS computation method, the cases needed for training and testing will be obtained with a relatively small time compared to using the traditional repeated simulation methods.

Note that the *RKE* calculation only needs one time domain simulation; meanwhile, the *DPE* for the particular MOD can be calculated off-line and be used on-line.

Therefore, one can use the proposed procedure to implement the on-line RAS calculation by splitting the above steps into off-line and on-line calculations:

- Off-line - calculate the *DPE* using steps 1) to 3).
- On-line calculate *RKE* using step 4) to 6).
- On-line determine the RAS action using step 7) and 8).

The communication and measurement infrastructure have a significant influence on the RAS implementation; in particular, it will affect the time availability for on-line computations. The ANN is promising for real-time adaptive RAS. Based on the proposed *RKE* and *DPE* calculation, one can select an ANN to directly output the sufficient RAS action, or use two ANNs for *RKE* and *DPE* separately, and then use criterion (3.6) to determine the RAS action. Such real time implementation needs further studies that are beyond the scope of this dissertation.

Still some practical issues that may be faced in the RAS implementation, whicwill be discussed in this dissertation. For example, time delay and different fault locations need to be considered in the off-line and on-line calculations. If detailed information for estimating a fault location is not available, the most conservative estimation has to be used for on-line decision. Frequency and phasor measurements can be used to detect the fault location. Again, estimating fault location is a different research topic from this dissertation.

3.2.3 Use hybrid method to calculate *RKE* and *DPE*

The hybrid method has been discussed in Chapter 2. It is used to estimate the transient energy from the time domain simulation results. In the hybrid method, the PEBS

is used to approximate the stability boundary. The residual kinetic energy at the PEBS crossing point is used as the energy margin of an unstable case. For a stable case, the kinetic energy will return to zero before the trajectory achieves the PEBS. The hybrid method first adds one or a series of pseudo faults at the time when the kinetic energy is zero. The pseudo faults are selected to cause the system to be critical unstable. Then the unstable equilibrium point following the pseudo faults can be used to estimate the PEBS crossing point. In the hybrid method, the energy margin for a stable case can be estimated by the difference between the injected kinetic energy and the residual kinetic energy at the PEBS crossing point plus a compensation for the position change along the trajectory caused by the pseudo faults.

The idea of the hybrid method is extended to the calculation of *RKE* and *DPE*. The procedure to calculate the *RKE* is to find the first local minimum corrected kinetic energy of an analysis case following the RAS action using the critical case as the reference. In (3.5), the *DPE* calculation needs to know the potential energy of the critical and reference cases. It can be replaced by estimation of energy margin by using the hybrid method. Two different *DPE* calculation methods are given in the next section.

3.3 Computational procedure of *DPE*

3.3.1 *DPE* computation using pseudo fault

Again consider the example given in Figure 3.1. There are two reference cases *cr* and *ca*, and one analysis case. A pseudo fault is added on the two selected reference cases. Then, the *DPE* can be approximated as the difference of the ability to absorb the kinetic energy injected by the pseudo fault between these two RAS reference cases. The

pseudo fault scenario (fault type, location and clearing time) can be the same as that which causes the system instability for the analysis case, or that has the clearing time slightly longer than the normal clearing time to ensure some margin.

Figure 3.2 gives a simple illustration of this idea. This figure is a modified version of Figure 3.1 where θ^a and θ^b are points in the angle space at the clearing time of the two reference cases *cr* and *ca*, respectively. Then θ^c is the point on the trajectory of case *ca* that has the same potential energy as the point θ^a, and θ^r is the point at the RAS time along the trajectory of the analysis case.

Given two reference cases with case *cr* the critical case (a case achieving the transfer limit or a case corresponding to the minimum required RAS action.) and a pseudo fault scenario, the procedure to calculate the *DPE* for the reference cases is as following:

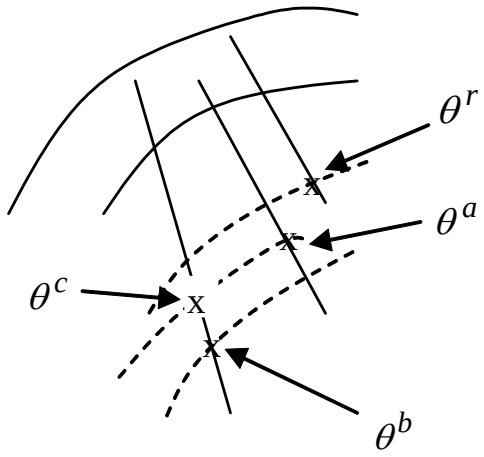

Figure 3.2 Estimating the *DPE* using pseudo faults

1) Add the pseudo fault on the reference cases and run time domain simulation.
2) If a case is stable, then use the hybrid method to calculate the positive margin V_{EM}, and let $V_i = V_{EM} + V_{KE}^{clr}$, ($i$ = 1 for case *cr*, i = 2 for case *ca*, V_{KE}^{clr} is the kinetic energy at the clearing point).
3) If a case is unstable, calculate $V_i = V_{KE}^{clr} - V_{KE}^{\min}$, where $V_{KE}^{\min}$ is the first local minimum kinetic energy, i.e., the kinetic energy at the point crossing the PEBS.
4) Calculate the compensation for PE between two cases DV_{pe} (discussed below).
5) Find the total different energy between two reference cases as: $DPE = V_2 - V_1 - DV_{pe}$.

The compensation of potential energy then is separated into two parts, one is the difference of PE between θ^a and θ^b called $PE(\theta^a, \theta^b)$, the other is the difference between $PE(\theta^r, \theta^a)$ and $PE(\theta^r, \theta^b)$. The trapezoidal method can be used to approximate the potential energy between two points if they are close to each other. That is, given *n* generators in the system and considering the angle and acceleration power as functions of time, then the PE difference is:

$$V_{PE} = -\frac{1}{2}\sum_{i=1}^{n}\left[P_{acci}(t_1) + P_{acci}(t_2)\right]\cdot\left[\theta_i(t_2) - \theta_i(t_1)\right] \qquad (3.7)$$

To compute the compensation of PE, two further approximations are used: one, using the acceleration power at θ^b, i.e., $P_{acc}(\theta^b)$, to approximate the acceleration power at θ^c, and two, using θ^a to approximate θ^c. Then from (3.1), the $PE(\theta^a, \theta^b)$ will be:

$$PE(\theta^a, \theta^b) = -\frac{1}{2}\sum_{i=1}^{n}\left[P_{acci}(\theta^b) + P_{acci}(\theta^b)\right]\cdot\left[\theta_i^a - \theta_i^b\right] \qquad (3.8)$$

As for the second part of the compensation of PE, it can be ignored if the point θ^r is not far apart from or lower than the clearing point of the pseudo fault for case *cr*. This assumption will hold if the clearing time for the pseudo fault is chosen carefully. For example, a longer clearing time of the pseudo faults for both case *cr* and *ca* can be used in order to obtain more conservative results.

Hence, the procedure to calculate the compensation for potential energy DV_{pe} is:

1) Record the angle vector (in the COA frame) in calculation of *DPE* for the two reference cases *cr* and *ca* at the clearing time.
2) Calculate the acceleration power of case *ca* at the clearing time using (2.7). Note that the value of the post-fault system is used.
3) Calculate the $PE(\theta^a, \theta^b)$ from (3.8).
4) Use the absolute value of $PE(\theta^a, \theta^b)$ to approximate DV_{pe}, which ensures a conservative estimate.

Alternatively, the EPEA curve can be used to approximate the compensation of the potential energy, in which the pseudo fault can use the normal clearing time. The procedure of the *DPE* computation using the EPEA curve is described in the next subsection.

3.3.2 *DPE* computation using the EPEA curve

The effect of a RAS action on an analysis case is illustrated in Figure 3.3. As mentioned in Chapter 2, the generation rejection will result in a sudden change in the

mechanical power of the generators and hence on the equivalent power of the OMIB system. Reflecting on the EPEA curve is that there is a sudden step down when a RAS action is taken. This change on the EPEA curve, caused by the RAS action, will increase the deceleration area seen in Figure 3.3. The calculation of *DPE* is illustrated by Figure 3.4. The same IEEE 39-bus test system and cases used in Chapter 4 have been used to obtain the curves on Figures 3.3 and 3.4. In this example, the operating points are expressed by the generation output of a generator, G_{35}. The operating point with G_{35}=460MW is the critical one for which the system is critically stable for the given fault scenario. At the operating point where G_{35}=540MW, a RAS action is needed following the given contingency. Following a RAS action, the original curve will drop down depending on how much generation has been reduced. As seen in Figure 3.4, reducing 140MW on G_{35} is sufficient to maintain the system stability, but 80MW is not.

To calculate the *DPE*, assume that the EPEA curve after a RAS action will be very close to the curve of the corresponding reference case. Then, the difference between the deceleration areas of the two reference cases approximates the *DPE*. Still, the closeness assumption may not hold due to the nonlinearity of the power system. This means the calculated *DPE* may be different from the increase of the deceleration area caused by the RAS action. Still, simulation results have shown that this mismatch will be canceled, or greatly reduced, since the *DPE* calculation is the difference of the two deceleration areas.

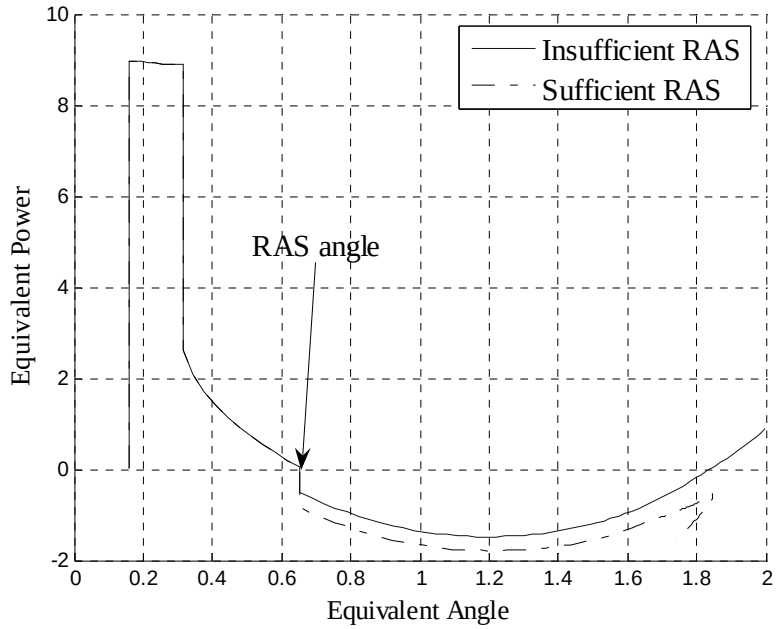

Figure 3.3 RAS actions observed on EPEA curves

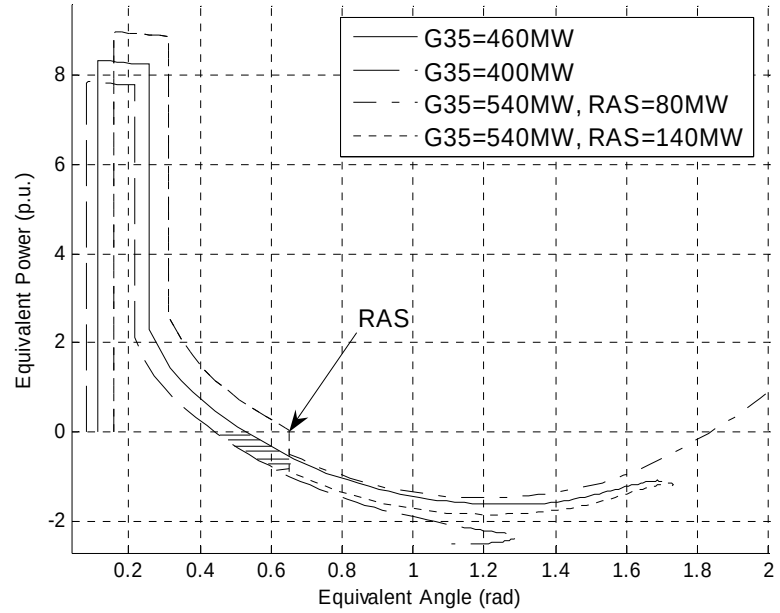

Figure 3.4 *DPE* calculations on EPEA curves

Then, the difference of the deceleration areas between the curves of the candidate and critical operating points approximates the *DPE*:

$$DPE = A_{dec}^{ca} - A_{dec}^{cr} - A_{comp} \tag{3.9}$$

where A_{dec}^{ca} and A_{dec}^{cr} are the deceleration areas for the candidate and critical operating points. The deceleration area can be obtained by either the Second Kick or the curve-fitting method. A_{comp} is the shadow area in Figure 3.4, which can be calculated by integration. Note that the *DPE* is the difference in the deceleration area after the angle corresponding to the RAS action. Hence, the *DPE* is not only a function of generation pattern, but also of the RAS angle.

For the computation of *DPE* on the curve, we need to estimate a probable range and generate an array of the RAS angles for the studied system and then calculate the *DPE* for all selected reference cases and all angles generated above. Moreover, at the same time as calculating the *RKE* for an analysis case, we need to record the RAS angle. A suitable reference case is determined by comparing the *RKE* and *DPE* for a specified RAS angle.

3.4 Robustness of RAS computation

Generally, the operating point at the transfer limit for transient stability is a convenient choice for the critical case. A good design method should give a conservative result for the transfer limit; however, different stability assessment methods may not give the same limit depending on the stability criterion and modeling accuracy. Therefore, the critical case may be unreliable when it is selected as the one with the transfer limit. On

the other hand, one may select the critical case away from the transfer limit to obtain a RAS approximation that is more conservative. Thus, it is important to determine whether the proposed RAS calculation method can tolerate the variation in the critical operating point.

There are some other factors that will affect the result of *RKE* calculation. For example, if other conditions are not changed, a delayed RAS action will result in a larger *RKE* hence a larger requirement of generation rejection. Similarly, when the fault location varies along the tie lines, the *RKE* will also be different. The robustness of the proposed method will be evaluated on the test systems in Chapter 4.

Chapter 4

SIMULATIONS OF ADAPTIVE RAS COMPUTATION

4.1 IEEE 39-bus system

4.1.1 System description

The IEEE 39-bus system, shown in Figure 4.1, is modified to be a two-area system such that the outlined area is the primary supply area and exports power to the remainder of the system. The tie lines between the areas are lines 16-17 and 16-15. Faults on these lines will create a severe disturbance in this system so that the system may separate into two groups in the first swing and require remedial action. (Note, a practical power system should survive all *N-1* contingencies, here for simplicity a single three-phase fault on these transmission lines leads to instability.) Only first swing instability is considered in the example.

Suppose in the demand area, the load at bus 18 is varied to create different operating points. The generation at bus 35, G_{35}, varies to balance the load at bus 18. For the three phase to ground fault on the transmission line from bus 16 to 17 located very close to bus 16, with fault clearing time of 0.1s, the transfer limit is G_{35} = 467 MW.

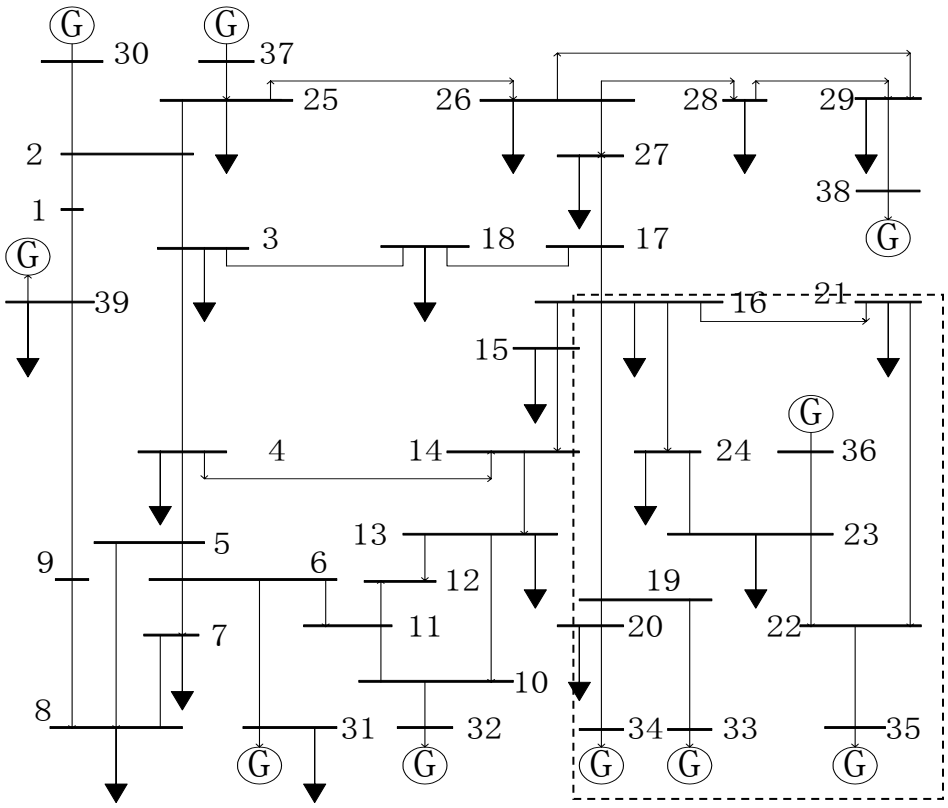

Figure 4.1 IEEE 39-bus system

The RAS will trip generation at a plant that is in the supply area and this plant will pick up all changes in the transfer power. Specifically, assume the RAS implements generator rejection at bus 35 that is balanced by load shedding at bus 18. For simplicity in this small system, it is assumed that either generation dropping or load shedding can be done in blocks of 20 MW. In a larger practical system, the amount would be determined by unit sizes and interruptible load. The maximum amount of a RAS action is the minimum of the generation at bus 35 and the load at bus 18.

4.1.2 RAS from pseudo fault method

4.1.2.1 RAS for different operating points

The example in this subsection illustrates the adaptive RAS for different operating points using the pseudo fault method. The fault is a three phase to ground fault on the transmission line from bus 16 to 17 located very close to bus 16, with fault clearing time of 0.1s The RAS actions occur at 0.2s after the fault (0.1s after the fault clears). The case with G_{35} = 460MW is used as the critical case. All cases with higher transfer power will require RAS actions since they will be unstable for the given fault scenario. The *RKE* of the unstable cases with respect to the critical case are listed in the Table 4.1. The *DPE* is calculated using a pseudo fault with 0.18s clearing time. *DPE* are calculated for seven reference cases and a 2nd order regression model is used to estimate the *DPE* for the other cases. The regression curves of the *DPE* and *RKE* are plotted in the Figure 4.2 and Figure 4.3. The *RKE* is zero when G_{35}=474 MW. That means when G_{35}=474 MW it is enough to reduce the generation down to 460MW to maintain the system stability.

Table 4.1 Generation of the supply area in IEEE 39-bus system

Bus	G_{33}	G_{34}	G_{35}	G_{36}
MW	502	508	Varying	500

Table 4.2 *RKE* of RAS analysis cases

G_{35}	740	720	700	680	660	640	620
RKE	1.567	1.452	1.354	1.246	1.135	1.033	0.921
G_{35}	600	580	560	540	520	500	480
RKE	0.803	0.685	0.571	0.447	0.322	0.185	0.029

Table 4.3 *DPE* of RAS reference cases

G_{35}	440	420	400	380	360	340	320
DPE	0.112	0.219	0.341	0.478	0.613	0.739	0.870

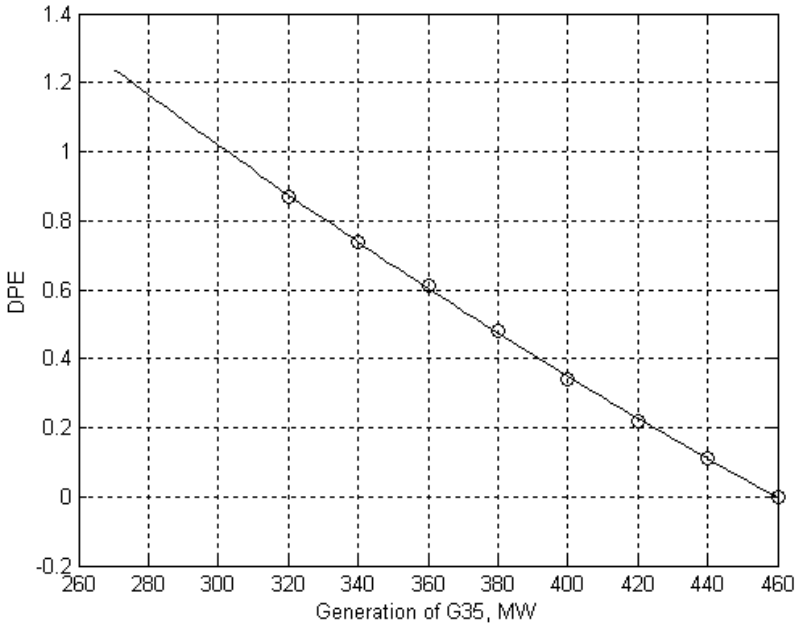

Figure 4.2 *DPE* of RAS reference cases

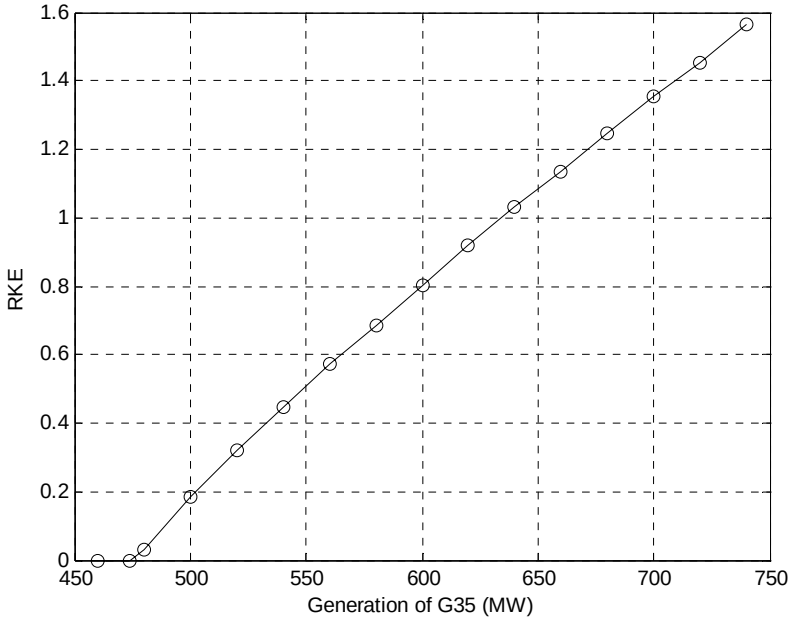

Figure 4.3 *RKE* vs. generation of G35

For a new unstable case, the RAS action can be determined by comparing the *DPE* and *RKE*. For example, given an operating point with G_{35} = 600MW, the *RKE* is 0.8, the RAS reference case whose *DPE* is greater than 0.8, is the case with G_{35} = 330MW. Then the RAS action is to shed load and drop generation equal to the difference, 270 MW. Complete results are given in the Table 4.4. It can be seen that the pseudo fault method provides conservative estimations for RAS requirements, if the system is first swing unstable. The errors are considered acceptable since these actions will only take place for extreme events, and in any case, would be less disruptive than the fixed schemes currently in use. For those operating points or faults that are not predefined, we can also find a RAS action by using the regression curves of *RKE* and *DPE*.

Table 4.4 RAS determination for different operating points of IEEE 39-bus system

G_{35} (MW)	L_{18} (MW)	RAS from proposed method		RAS from repeated simulation
		Figure 4.2 & 4.3	Rounded to 20 MW block	
700	430	>430	>430	420
680	410	>410	>410	380
660	390	377	380	340
640	370	343	360	305
620	350	307	320	270
600	330	270	280	235
580	310	233	240	217
560	290	195	200	165
540	270	156	160	130
520	250	116	120	95
500	230	73	80	60
480	210	26	40	30[1]

Using the pseudo fault method of *DPE* calculation, the selection of the clearing time of the pseudo fault has a significant effect on the result. Generally, a rough range for this clearing time is between the normal clearing time and the RAS time. Simulation results show *DPE* will be more conservative as the clearing time is larger, hence the result of RAS will be very conservative if a large clearing time is used. Several trials might be needed to select an appropriate clearing time. Table 4.5 shows the effects of the change in the clearing time of the pseudo fault to the results of RAS calculation.

[1] If RAS < 30MW, the system has negative damping.

Table 4.5 Effect of the clearing time of the pseudo fault to RAS computation

Operating points G_{35} (MW)	RAS by pseudo fault with 0.18s clearing time	RAS by pseudo fault with 0.16s clearing time	RAS from numerical simulation
700	>430	406	420
680	>410	376	380
660	377	344	340
640	343	314	305
620	307	282	270
600	270	248	235
580	233	215	200
560	195	181	165
540	156	145	130
520	116	108	95
500	73	69	60
480	26	25	30[2]

4.1.2.2 RAS for different fault locations

In this test, the RAS actions for different fault locations along the transmission line from bus 16 to 17 are determined by the proposed method. Again, the faults are three phase to ground faults. The clearing time (neglecting that clearing time may change with the fault in order to simplify the comparison) and RAS initiated time remain the same. The generation output in the supply area of the analysis case is listed in Table 4.6. Note that in this example, the generation dispatch pattern is different from the example in the previous subsection.

The analysis case itself is selected as the critical case. The *RKE* for different fault locations are given in Table 4.7. The *DPE* is calculated similarly to example 1, but the

[2] If RAS < 30MW, the system has negative damping.

clearing time for the pseudo fault is 0.13s. *DPE* are calculated only for the 11 RAS reference cases (in Table 4.8) and a 2nd order regression model is used to estimate the *DPE* of other RAS reference cases. Then for different fault locations, the RAS action can be determined by comparing the *DPE* and *RKE*. These results are given in the Table 4.9. Table 4.10 shows the effects of the change in the clearing time of the pseudo fault to the results of RAS calculation.

Table 4.6 Generation of the supply area

Bus	G_{33}	G_{34}	G_{35}	G_{36}
MW	650	500	600	400

Table 4.7 *RKE* for different fault locations w.r.t. G_{35}=600MW

% to bus 16	1	10	20	30	40	50
RKE	2.091	1.586	1.208	0.963	0.765	0.615
% to bus 16	60	70	80	90	99	
RKE	0.477	0.347	0.218	0.086	0.005	

Table 4.8 *DPE* of RAS reference cases w.r.t. G_{35}=600MW

G_{35}	580	560	540	520	500	480
DPE	0.057	0.135	0.199	0.274	0.373	0.463
G_{35}	460	440	420	400	380	
DPE	0.591	0.740	0.847	1.02	1.17	

Table 4.9 RAS Determination for different fault locations

Fault location (% to bus 16)	RAS from proposed method (Rounded to 20 MW block)	RAS from simulation (MW)
1	320	320
10	280	225
20	240	175
30	200	145
40	180	125
50	160	115
60	120	100
70	100	90
80	80	80[b]
90	40	70[b]
99	20	65[b]

Table 4.10 Effect of the clearing time of the pseudo fault to RAS computation

Fault location (% to bus 16)	RAS by pseudo fault with 0.13s clearing time	RAS by pseudo fault with 0.15s clearing time
1	320	380
10	280	340
20	240	280
30	200	260
40	180	220
50	160	200
60	120	160
70	100	140
80	80	100
90	40	60
99	20	20

[b] The system has negative damping if the RAS is less than the given value.

In this example, the *DPE* for G_{35} < 380MW have been extrapolated from the data in Table 4.8 to obtain the RAS for the fault location very close to the bus. The *DPE* obtained in such way may be different from the values directly calculated using the proposed method, hence the RAS may also different. For example, the RAS for this fault 1% away from Bus 16 will be 360MW if using the *DPE* calculated by the proposed method. Still, some cases lose stability due to negative damping when using the proposed method to determine the RAS. For these cases, small signal analysis is necessary.

As discussed in Chapter 3, the *DPE* is not only a function of the operating points, but also a function of the equivalent angle where the RAS is taken. Hence, the *DPE* curve is a 3-dimensional curve. Using the pseudo fault method is actually equivalent to selecting the maximum possible equivalent angle where the RAS is taken. Hence, the *DPE* curve is projected to a 2-dimensional curve with only the *DPE* axis and the operating point axis. Using the 2-dimensional *DPE* curve can reduce the burden of on-line decision compared to using the 3-dimensional *DPE*, but the off-line calculation will be increased because of the simulations for pseudo faults and the accuracy may be also reduced.

4.1.3 RAS from the EPEA curve

In this subsection, the EPEA curve will be used to calculate the RAS. The fault scenario and the RAS time and location are the same as used in Subsection 4.1.2. The generation dispatch is also the same as in Table 4.1. The operating point with G_{35} = 460 MW is the critical case. So that, the *RKE* are still the same as in Table 4.2 and the curve of *RKE* versus generation of G_{35} is the same as in Figure 4.3. To use the EPEA curve, we also need to know the equivalent angle when the RAS is initiated for all operating points

with higher transfer power than the transfer limit. The *RKE* and the equivalent angle are listed in the Table 4.11.

Table 4.11 *RKE* and RAS angles of analysis cases

G_{35}	740	720	700	680	660	640	620
RKE	1.567	1.452	1.354	1.246	1.135	1.033	0.921
RAS angle	0.859	0.838	0.817	0.796	0.775	0.754	0.734
G_{35}	600	580	560	540	520	500	480
RKE	0.803	0.685	0.571	0.447	0.322	0.185	0.029
RAS angle	0.714	0.693	0.672	0.652	0.631	0.611	0.590

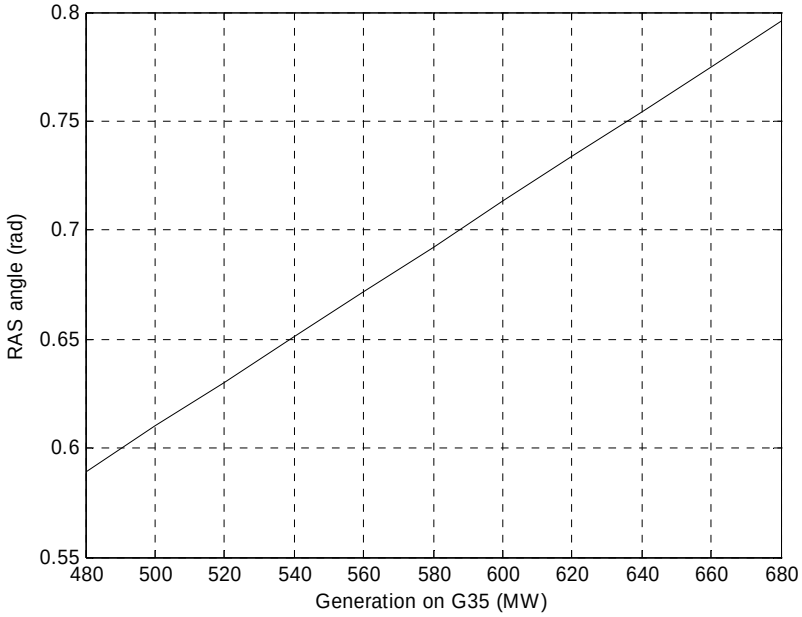

Figure 4.4 Equivalent angles when RAS is initiated

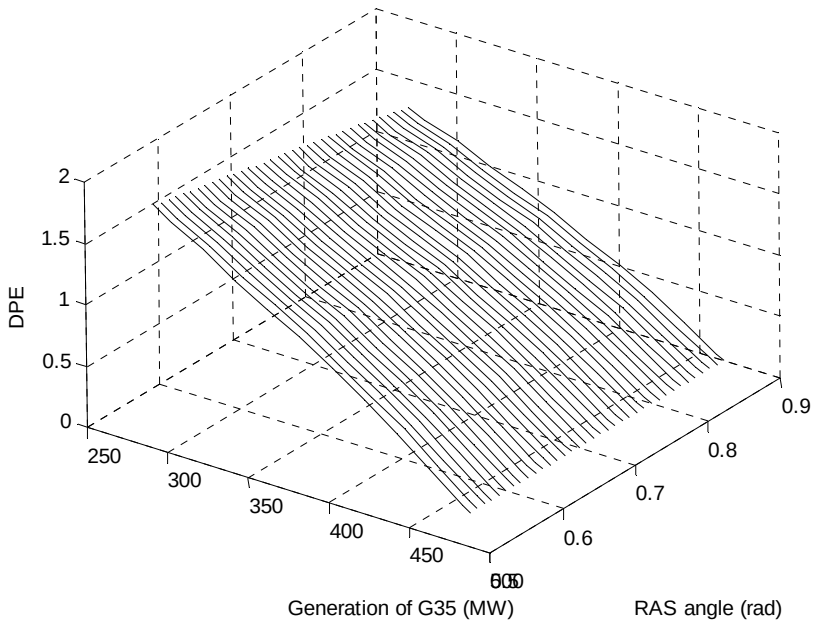

Figure 4.5 *DPE* as the function of generation of G_{35} and the RAS angle

Using the EPEA curve, a 3-dimensional graph of the *DPE* can be plotted as in Figure 4.5. This graph of *DPE* is calculated once and can be reused to determine the RAS action for any of the unstable cases whose transfer power is higher than the transfer limit.

The RAS can be calculated graphically on Figure 4.3, Figure 4.4 and Figure 4.5. For example, for the case with G_{35} = 600 MW, the *RKE* is 0.8 and the RAS angle is 0.714. To determine the RAS action, we select an angle that is a slightly greater than 0.714, say 0.72, to be conservative. Then we select a reference case whose *DPE* is greater than 0.8 for the selected angle. In this example, the suitable reference case is the case of G_{35} = 360 MW and the RAS action is to shed load and drop generation equal to the difference, i.e., 240 MW. Complete results for RAS are given in Table 4.12. This table shows that the RAS calculation using the Second Kick can provide conservative estimates for RAS. On

the other hand, using curve-fitting may give the inadequate generation rejection since the calculated energy margin is overly optimistic comparing to the second kick method, as shown in Figure 2.8. Therefore, the Second Kick method is more effective for *DPE* calculation. Still, since the curve-fitting calculation is faster than the Second Kick, it may be used as a starting point for some applications, e.g., a fast update of a database or look-up table. The resulting comparison of RAS computations is also illustrated in Figure 4.6 with respect to the generation of G_{35}.

Table 4.12 Results of RAS from EPEA curve

G_{35} (MW)	L_{18} (MW)	RAS from proposed method		RAS from repeated simulations
		Using second kick	Using curve- fitting	
700	430	>430	>430	420
680	410	400	380	380
660	390	360	340	340
640	370	320	300	305
620	350	280	260	270
600	330	240	220	235
580	310	200	200	200
560	290	180	160	165
540	270	140	120	130
520	250	100	100	95
500	230	60	60	60
480	210	40	40	30

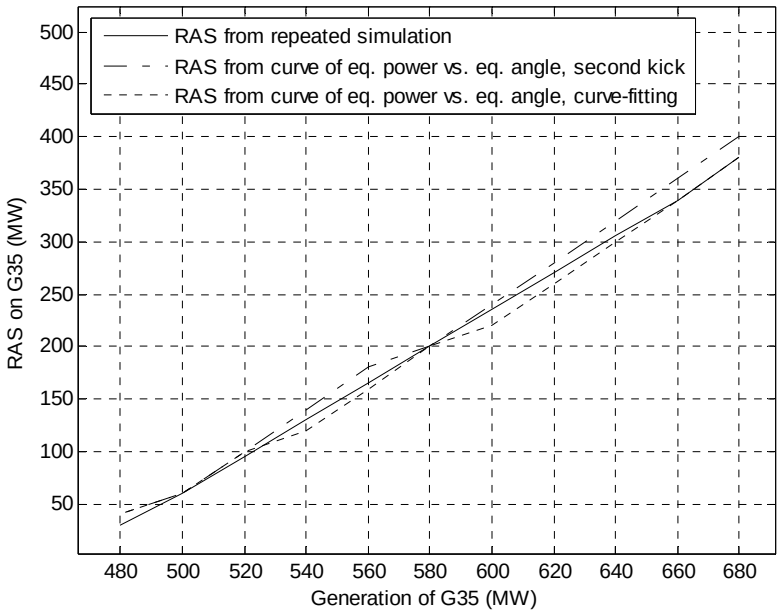

Figure 4.6 RAS vs. generation of G_{35}

4.1.4 Robustness of RAS calculation for the critical cases

Generally, the operating point at the transfer limit for transient stability is a convenient choice for the critical case; however, different stability assessment methods may not give the same limit depending on the stability criterion and modeling accuracy. One may also select the critical case away from the transfer limit to obtain a RAS approximation that is more conservative. Therefore, the critical operating point may be variable. The robustness to the variation of the critical operating points will be evaluated in this subsection on the IEEE 39-bus system.

In Subsection 4.1.4, the case with G_{35}=460 MW is selected as the critical one. To test the robustness of the proposed method to the variation in the critical case, several different operating points around G_{35}=460 MW are used for the RAS calculation. For example, the operating point with G_{35}=465 MW is still stable, but closer to the transfer

limit G_{35}=467 MW, which is obtained from repeated time domain simulation. For the given fault scenario in Subsection 4.1.2, the energy margins from the Second Kick method are 0.0410 and 0.1084, respectively, for the G_{35}=465 MW case and the G_{35}=460 MW case.

For different critical cases, the *RKE* and *DPE* need to be recalculated. For example, Figure 4.7 and Figure 4.8 show the *RKE* and *DPE* using the case G_{35} = 465 MW as the critical cases. Only the *RKE* of unstable cases with G_{35} equal to or less than 680 MW are plotted in Figure 4.7. The complete results of the RAS calculations are listed in Table 4.13, where all operating points are expressed by the generation output of G_{35}. With different critical cases, the proposed method can provide very similar results for RAS requirement, and all of these results are conservative.

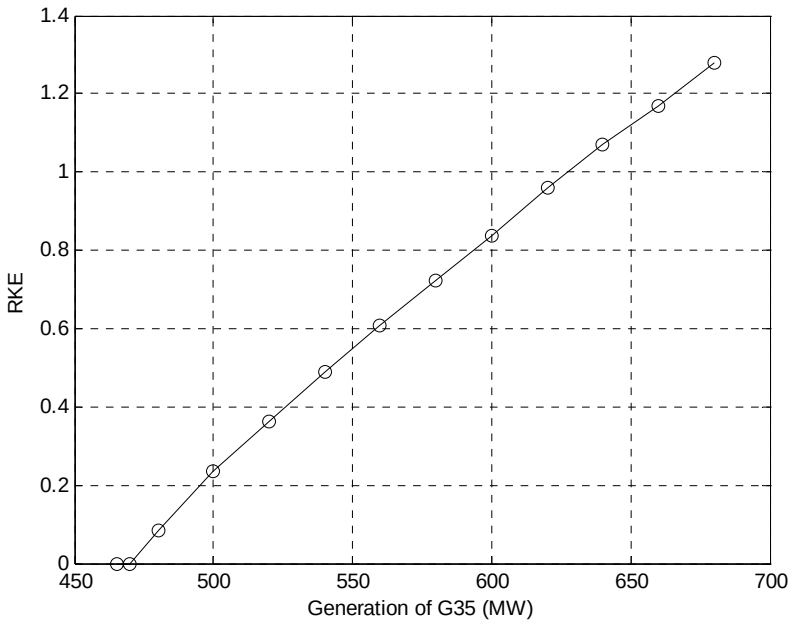

Figure 4.7 *RKE*, critical case with G_{35} = 465 MW

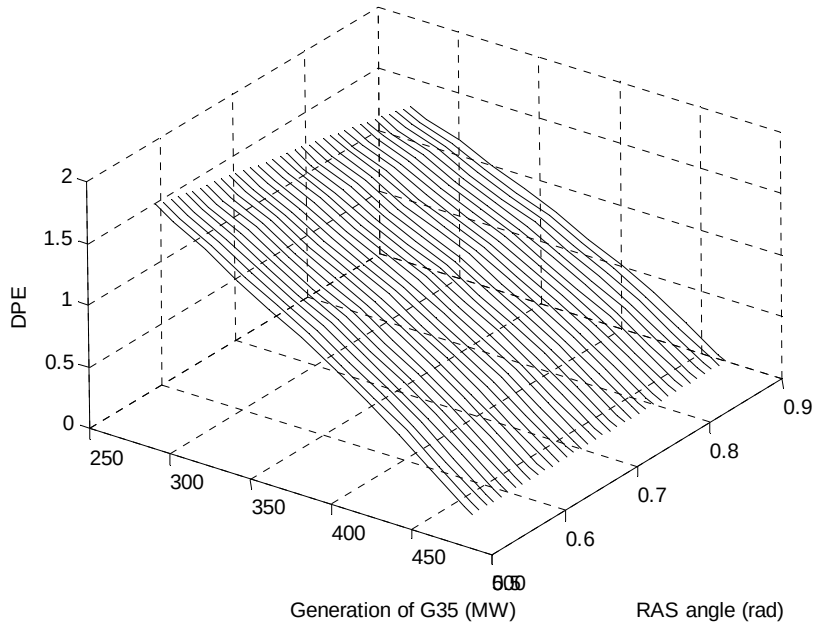

Figure 4.8 *DPE*, critical case with G_{35} = 465MW

Table 4.13 Robustness to critical case variation

G_{35} (MW)	RAS from the different critical cases (cr)			
	cr: G_{35}=465	cr: G_{35}=450	cr: G_{35}=440	cr: G_{35}=460
680	400	400	400	400
660	360	360	360	360
640	320	320	320	320
620	280	280	280	280
600	240	240	240	240
580	200	200	220	200
560	180	180	180	180
540	140	140	140	140
520	100	100	100	100
500	60	60	60	60
480	40	30	40	40

4.1.5 Variable RAS initiation time and fault location

For a given RAS location, the calculated *DPE* can be reused when the RAS initiated time is variable but the topology of the system is not changed following the RAS action. To determine the new RAS requirement, one only needs to calculate the *RKE* under the new RAS initiation time. Similarly, if the fault location is varied along the transmission line, then only the *RKE* needs to be recalculated. Table 4.14 uses two examples to show that the proposed method can be applied for variable RAS initiation time and fault locations. As in subsection 4.1.4, the critical operating point is G_{35}=460 MW. In the first example, the RAS initiation time is changed from 0.2s to 0.22s. In the other example, the fault location is changed from 1% to 10% away from bus 16, but the RAS initiation time is still 0.2s. In Table 4.14, Adap. RAS indicates the RAS from the proposed method while Re-sim RAS indicates the RAS from the repeated time domain simulations. Compard with the benchmark, the delayed RAS requires rejecting more generation on G_{35} since *RKE* increases; when the fault location is farther away from bus 16, the requirements of RAS will reduce since *RKE* decreases. For both examples, only the *RKE* are recalculated, the *DPE* is directly obtained from Figure 4.5.

The *RKE* is plotted in Figure 4.9 as well as the *RKE* of the cases with 0.2s RAS and fault 1% away from bus 16 that are used as the benchmarks. The results of RAS computation for the benchmark are also listed in Table 4.14, which is the same as the results from the Second Kick method in Table 4.12.

Table 4.14 RAS for delayed RAS and different fault locations

G_{35} (MW)	Delayed RAS action (0.22s)		Different Fault location (10% from bus 16)		Benchmark (0.2s RAS, fault 1% from bus 16)	
	Adap. RAS	Re-sim RAS	Adap. RAS	Re-sim RAS	Adap. RAS	Re-sim RAS
680	410	405	300	285	400	380
660	380	365	260	245	360	340
640	340	325	240	220	320	305
620	300	290	200	190	280	270
600	260	250	160	155	240	235
580	220	210	140	125	200	200
560	180	175	100	95	180	165
540	140	135	80	60	140	130
520	100	100	60	30	100	95
500	80	65	40	0	60	60
480	40	30	20	0	40	30

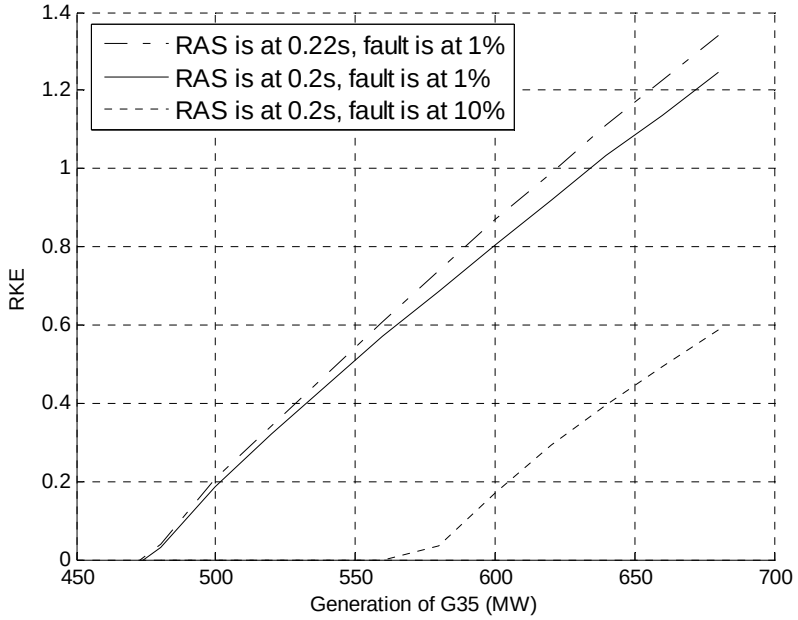

Figure 4.9 *RKE* comparison

4.1.6 Robustness to variable fault clearing time

In a real power system, the fault clearing time may vary according to operating point, fault location, fault type and protective relay schemes [44]. For example, if a transmission line is protected by distance relay and there is a communication link between the relays on both sides of the line, the primary relays on both sides can trip the fault occurring on the line without any intended delay. For this relay scheme, clearing time for faults occurring at different locations on the line can be considered very similar to each other (with up to perhaps have 0.4 cycle deviations [44]). Other relay schemes may have different clearing times dependent on the different fault locations, for example, over-current relay or some backup relays that use the inverse-time over-current relay as the timer. The time settings of these relays are dependent on the actual operating conditions of the system. Therefore, the robustness of the proposed RAS calculation to the variation of the fault clearing time needs to be evaluated. Note the backup relays, which are either the zone 2 or zone 3 relay, or the backup for breaker failure, may cause tripping of different lines or other devices, which will cause the topology change from the assumed topology for the RAS calculation. That requires the coordination between the RAS and the regular protection schemes, as well as with other RAS. The coordination issue is not further discussed in this dissertation. The examples given in this subsection will illustrate that the proposed method is robust to variable fault clearing times.

Table 4.15 shows the RAS for a given operating point with the varying fault clearing time. In this example, the operating point is that G_{35}=600 MW; the fault is 10% away from bus 16. Figure 4.10 shows the relationship between the equivalent angles when the RAS is initiated versus the equivalent angles when the fault is cleared. Figure

4.11 shows the relationship between the *RKE* and the equivalent angles when the fault is cleared. Using these curves, one can estimate the *RKE* and the equivalent angle when the RAS is taken by monitoring the angles immediately following the fault clearing.

Table 4.15 RAS for different fault clearing times, given operating point

Clearing time (s)	RAS time (s)	Adap. RAS (MW)	Re-sim RAS (MW)
0.08	0.18	140	105
0.09	0.19	140	130
0.1	0.2	160	155
0.11	0.21	200	190
0.12	0.22	240	225
0.13	0.23	280	265
0.14	0.24	>330	315

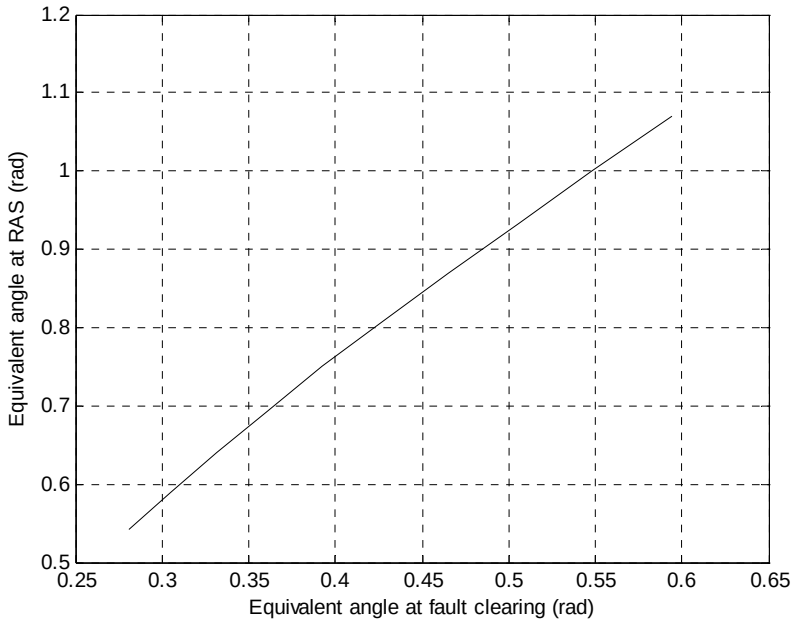

Figure 4.10 Eq. angles at fault clearing vs. Eq. angle at RAS

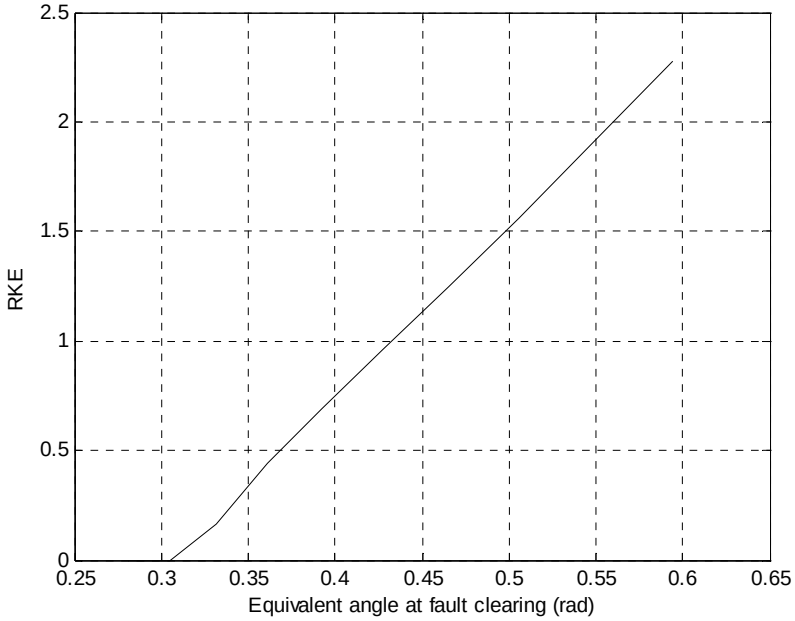

Figure 4.11 Eq. angles at fault clearing vs. *RKE*

Table 4.16 shows the results of RAS calculation for different operating points, different fault locations and different fault clearing time. The proposed adaptive computation still gives conservative results comparing to repeated simulations. It shows that the adaptive computation method is robust to different fault clearing time. For the examples given in this subsection, we only need to recalculate the *RKE* curve for the new faults (different location and clearing time). The *DPE* curves originally obtained in subsection 4.1.4 can still be used. Thus, the computation burden for calculating the new RAS amount is small.

Table 4.16 RAS for different fault clearing time, different operating points

G_{35} (MW)	L_{18} (MW)	10% fault, 0.12s clearing, 0.22s RAS		1% fault, 0.08s clearing, 0.18s RAS	
		Adap. RAS	Re-sim. RAS	Adap. RAS	Re-sim. RAS
680	410	400	375	280	275
660	390	360	335	260	245
640	370	320	300	220	215
620	350	260	260	200	185
600	330	240	225	160	155
580	310	200	190	140	125
560	290	160	150	100	95
540	270	120	115	80	60
520	250	80	80	60	30
500	230	60	45	40	0
480	210	20	10	20	0

4.2 WECC 179-bus system

4.2.1 System description

A 179-bus model as a simplified representation of the WECC system is now studied by the presented adaptive RAS calculation method. A one-line diagram of the system is given in Figure 4.12. Along the transmission path from bus 76 to 82, which corresponds to the path between large hydro stations in the Northwest and loads in California, the system is configured as a two-area system. The north of bus 76 is the primary supply area that includes six generators at busses 30, 35, 65, 70, 77, and 79. The system is weakened by stretching the transmission lines between bus 76 and 82, so that two line outages may be severe enough to separate the system into two groups along this transmission path in

the first swing. A detailed dynamic model can be used since the time domain simulation is applied to obtain the system response; however, the governor is not included so that the mechanical power input is only changed by generation rejection.

Similar to the simulations on the IEEE 39-bus system in the previous section, the RAS will trip generation at a plant that is in the supply area. The generator rejection is balanced by load shedding at buses in the demand area, although this may not be necessary if the demand area has sufficient reserves. For simplicity, when applying the proposed method, it is assumed that either generation dropping or load shedding can be done in blocks of 100 MW. In a practical system, the amount would be determined by unit sizes and interruptible load. The maximum amount of a RAS action is the minimum of the generation and the load at selected busses.

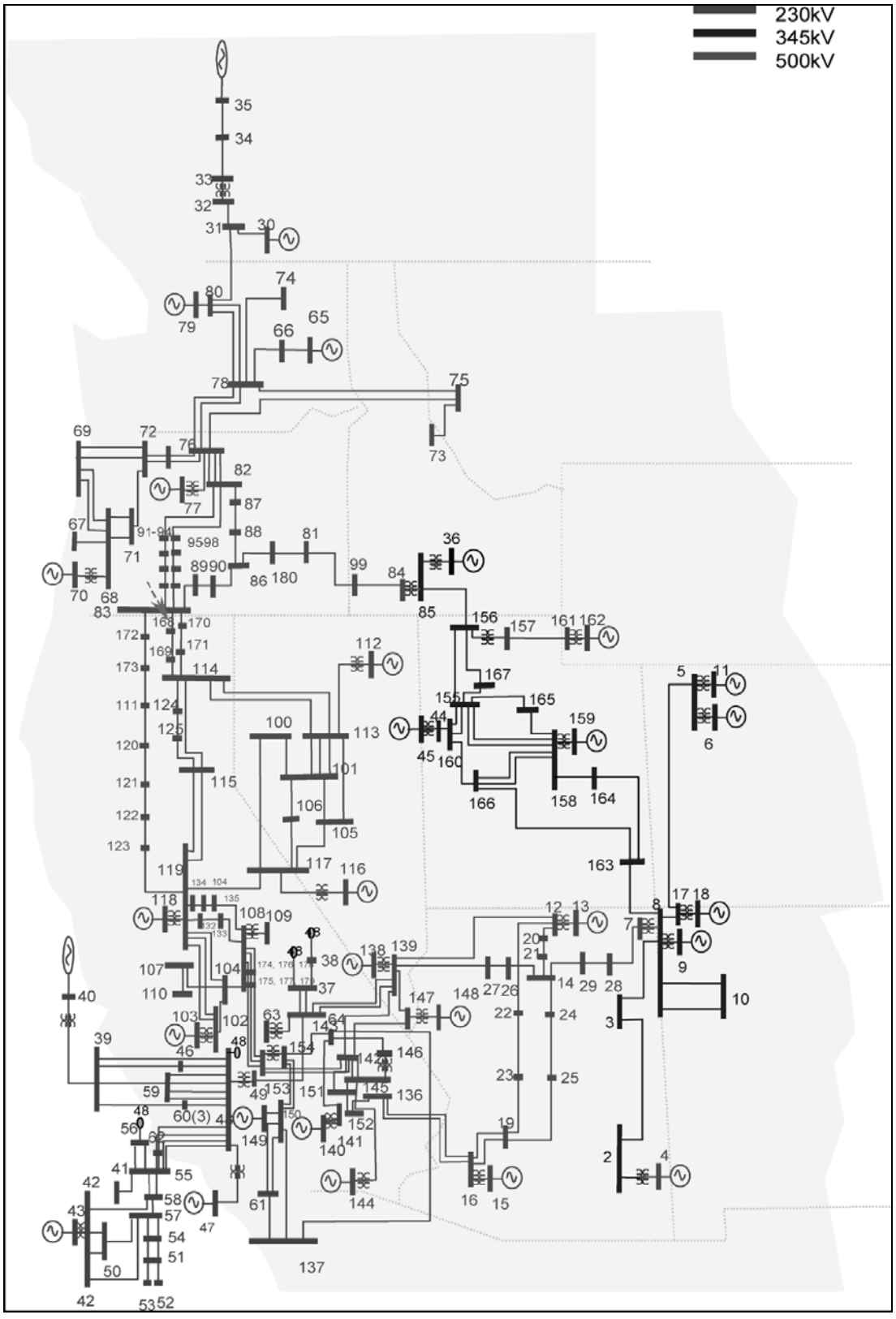

Figure 4.12 WECC 179bus system (reprinted from [43])

4.2.2 RAS for different operating points

Suppose in the demand area, the load at bus 150, located in Southern California, is varied to create different operating points. The generation at bus 77 in the Northwest, G_{77}, is used to balance the load. A 3-phase to ground fault, located very close to bus 76, occurs on one of three parallel transmission lines from the Northwest. The fault is cleared in 0.1 seconds by removing the faulted line. Simultaneously, another parallel line along this path is removed to simulate an N-2 contingency. The RAS action is initiated at 0.1s after the fault clears. When G_{77} is 3200 MW, the transfer power reaches its transient stability limit for the given fault scenario.

The case at the transfer limit is the critical case. All cases with higher transfer power than the critical case require RAS actions since they are unstable for the given fault scenario. The *DPE* is calculated by using the EPEA curve. We obtain the 3-dimensional graph of the *DPE* shown in Figure 4.13. Curves of *RKE* and angles at the time when the RAS is initiated versus the generation output are plotted in Figure 4.14 and 4.15.

The RAS can be determined graphically from Figure 4.13, Figure 4.14 and 4.15. For example, for the case with G_{77} = 4400 MW, the *RKE* is 2.210 and the RAS angle is 1.589. To determine the RAS action, we select an angle that is a slightly greater than 1.589, say 1.600, to be conservative. Then we select a reference case whose *DPE* is greater than 2.210 for the selected angle. In this example, the suitable reference case is the case where G_{77} = 2800 MW and the RAS action is to shed load and drop generation equal to the difference, i.e., 1600 MW. Note if *RKE*=0, then the RAS is the difference in generation between the unstable case and the critical case, e.g., the case with G_{77}=3600MW has a zero *RKE* and the critical case has G_{77}=3200MW then the sufficient RAS for this case is

400MW. Complete results are given in Table 4.17, where the column denoted Re-sim RAS is the control obtained from repeated time domain simulation, while the column denoted as Adap. RAS is from the proposed adaptive computation method. The first two columns of Table 4.17 are the load and generation at bus 150 and 77, respectively.

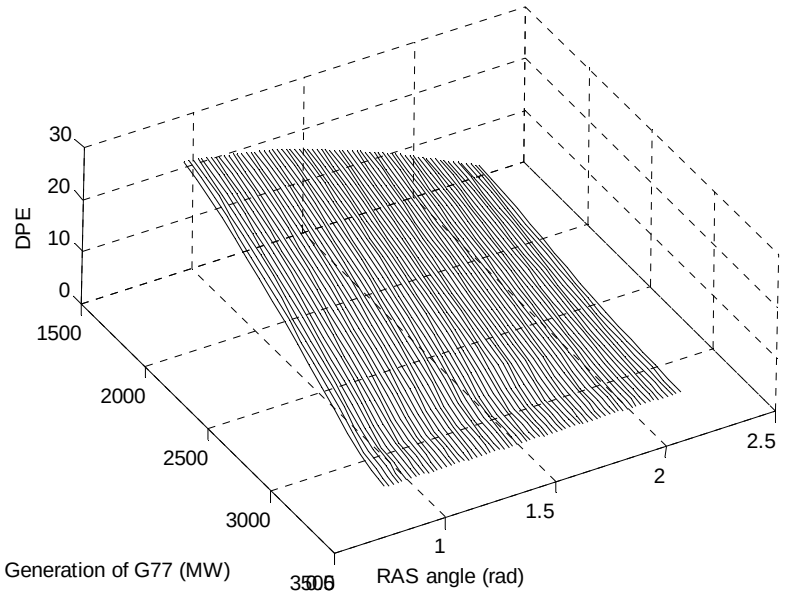

Figure 4.13 *DPE* as the function of generation of G_{77} and the RAS angle

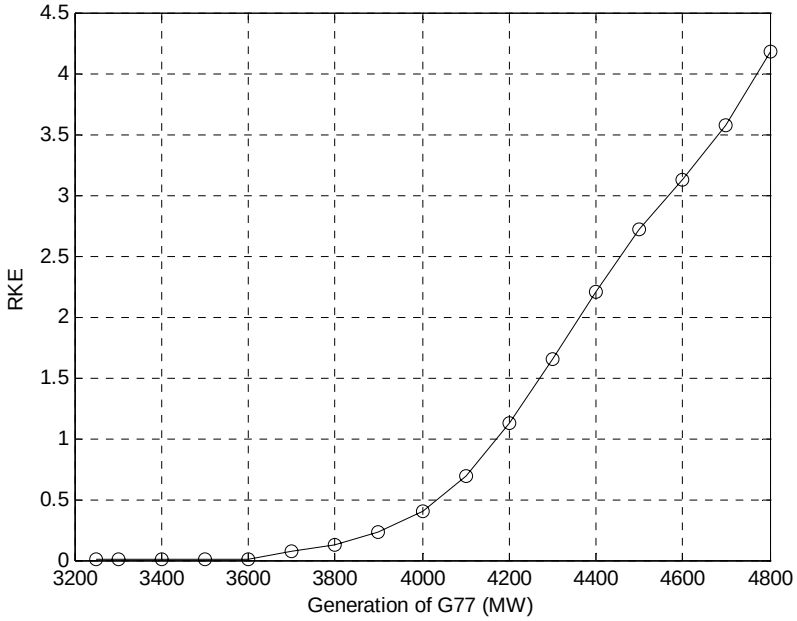

Figure 4.14 *RKE* of RAS analysis cases

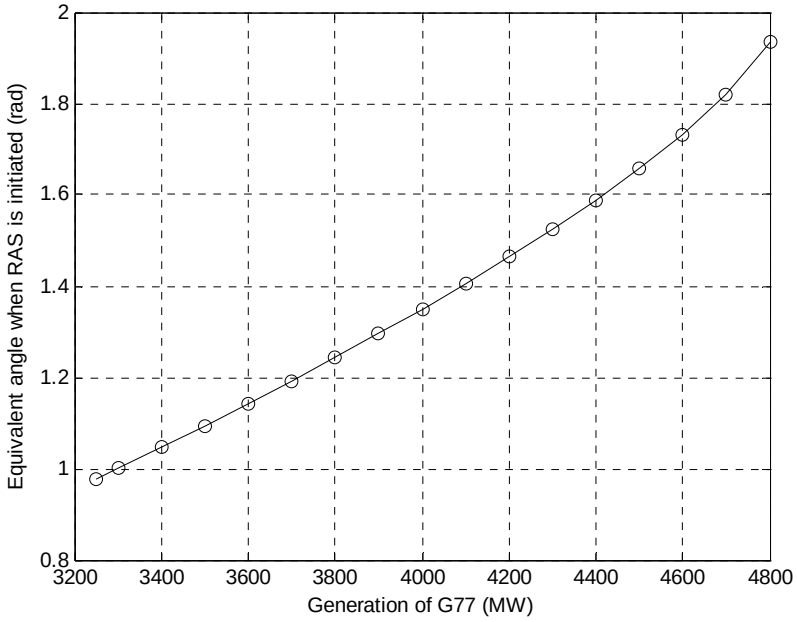

Figure 4.15 Equivalent angles when RAS is initiated

Table 4.17 RAS for different operating points (WECC 179-bus)

Load at bus 150 (MW)	Generation at bus 77 (MW)	Re-sim. (MW)	Adap. RAS (MW)
3250	3250	50	50
3300	3300	100	100
3400	3400	200	200
3500	3500	300	300
3600	3600	400	400
3700	3700	550	550
3800	3800	650	650
3900	3900	750	750
4000	4000	900	900
4100	4100	1000	1100
4200	4200	1150	1300
4300	4300	1300	1400
4400	4400	1450	1600
4500	4500	1600	1700
4600	4600	1750	1800
4700	4700	1950	2100
4800	4800	2250	2300

4.2.3 Robustness with respect to variation of critical cases

In the previous example, the critical case corresponds to G_{77} = 3200 MW and L_{150} = 3200 MW. It is important to determine if the proposed method is robust to variations in these conditions. Using a similar scenario as the previous, but changing the critical case, Table 4.18 demonstrates the robustness of the proposed method to variation of the critical cases. In these examples, the calculated RAS amounts are all still conservative.

Table 4.18 Robustness to critical case variation (WECC 179-bus)

G_{77} (MW)	Re-sim RAS (MW)	Adap. RAS (MW)			
		Critical case: G_{77} = 3200MW	Critical case: G_{77} = 3150MW	Critical case: G_{77} = 3100MW	Critical case: G_{77} = 3000MW
3250	50	50	100	150	250
3300	100	100	150	200	300
3400	200	200	250	300	400
3500	300	300	350	400	500
3600	400	400	450	500	600
3700	550	550	550	600	700
3800	650	650	650	700	800
3900	750	750	750	800	900
4000	900	900	900	900	1000
4100	1000	1100	1000	1000	1100
4200	1150	1300	1200	1200	1200
4300	1300	1400	1400	1400	1300
4400	1450	1600	1600	1500	1500
4500	1600	1700	1700	1700	1600
4600	1750	1800	1800	1800	1800
4700	1950	2100	2000	2000	2000
4800	2250	2300	2300	2400	2400

4.2.4 Robustness to variation in location of RAS actions

Another concern for the RAS determination is that the location of a control action may need to change because of some operating issues, e.g., due to contracts of interruptible load or water conditions in hydro plants, and so on. To determine the robustness of the proposed method to variable locations, we use the same fault scenario as in the previous example, but the operating points are created by varying load and

generation at different busses. The RAS actions are also initiated at these busses. Then, the proposed method is used to determine the RAS for the new locations. Both the *DPE* and *RKE* need to be recalculated since the control location changes. The results of the RAS calculation are listed in Table 4.19 for two examples with different locations of RAS actions as described in Table 4.20.

Table 4.19 RAS for variable RAS locations (WECC 179-bus)

#	Example 1			Example 2		
	Case (G_{77})	Re-sim. RAS	Adap. RAS	Case (G_{79})	Re-sim. RAS	Adap. RAS
1	3250	50	50	7350	50	50
2	3300	100	100	7400	100	100
3	3400	200	200	7500	200	200
4	3500	300	300	7600	300	300
5	3600	400	400	7700	400	400
6	3700	500	500	7800	500	500
7	3800	600	600	7900	650	650
8	3900	700	700	8000	750	750
9	4000	800	800	8100	850	850
10	4100	900	900	8200	1000	1000
11	4200	1000	1000	8300	1100	1200
12	4300	1150	1150	8400	1250	1400
13	4400	1250	1250	8500	1400	1600
14	4500	1400	1400	8600	1600	1700
15	4600	1500	1600	8700	1750	1800
16	4700	1650	1800	8800	1950	2000
17	4800	1800	2000	8900	2250	2300

Table 4.20 Description of examples for variable location of RAS actions

#	RAS location	Critical case
1	Generator bus: 77, Load bus:119	G_{77} = 3200MW, L_{119}=3000MW
2	Generator bus: 79, Load bus: 150	G_{79} = 7300MW, L_{150}=3200MW

4.2.5 Variable RAS initiation time and fault location

For a given RAS location, the calculated *DPE* can be reused when the RAS initiated time is variable since the topology of the system is not changed following the RAS action. To determine the new RAS requirement, one only needs to find the *RKE* under the new RAS initiation time. This process is similar to where the fault location is varied along the transmission line. *RKE* versus generation at bus 77 for the different RAS initiated time and different fault location are plotted on Figure 4.16, as well as the *RKE* used in Subsection 4.2.2 for comparison.

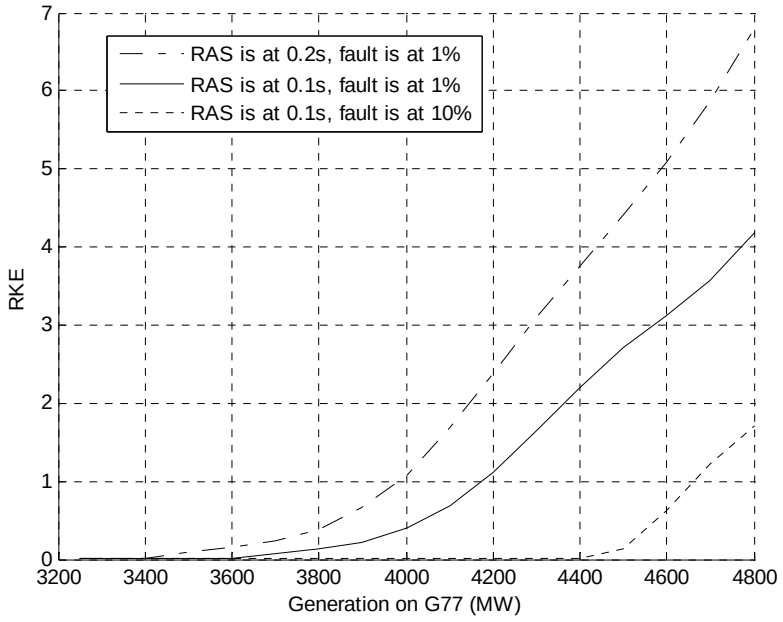

Figure 4.16 *RKE* comparisons for WECC 179-bus system

Table 4.21 RAS for different RAS initiated time and fault locations (WECC 179-bus)

G_{77} (MW)	RAS initiated time: 0.3s		Fault Location: 10%	
	Re-sim. RAS	Adap. RAS	Re-sim. RAS	Adap. RAS
3250	50	50	50	50
3300	100	100	100	100
3400	200	250	200	200
3500	300	350	300	300
3600	400	450	400	400
3700	550	550	500	500
3800	700	700	600	600
3900	800	900	700	700
4000	950	1100	800	800
4100	1100	1200	900	900
4200	1300	1400	1000	1000
4300	1450	1500	1100	1100
4400	1650	1700	1200	1200
4500	1850	2000	1350	1400
4600	2100	2200	1500	1600
4700	2400	2500	1650	1800
4800	2750	3100	1850	2000

Table 4.21 shows two examples where the proposed method remains effective across variable RAS initiation time and fault location. Again, the load and generation dropping occurs at bus 150 and 77, respectively, and the critical case is the one with G_{77}=3200 MW. In the first example, the RAS time is delayed from 0.2s to 0.3s following the fault clearing. In the other example, the fault location is moved further down the line (10% along the path from bus 76 to bus 82), but the RAS still acts at 0.2s. For both examples, only the *RKE* is recalculated. The *DPE* is directly obtained from the previous example.

Comparing with Table 4.17, the delayed RAS requires greater generation rejection due to the *RKE* increase. When the fault location is further down the line and thus less severe, the generation reduction is reduced.

In the next example, variable RAS intiation time are used for the case that has the operating point G_{77}=4800 MW, L_{150}=4800MW and the fault location is 1% way from bus 77, fault clearing time is 0.1s. The critical operating point for this given fault scenario is G_{77}=3200 MW, L_{150}=3200 MW. The RAS initiated time varies from 0.1s to 0.2s after the fault clearing by 0.01s step size. Table 4.22 listed the results of RAS computation. Figure 4.17 shows the curve of the *RKE* versus the equivalent angle where the RAS is taken. It can be seen that there is a near-linear relationship between the *RKE* and the RAS angle.

Table 4.22 RAS for variable RAS initiated time (WECC 179-bus)

RAS initiated time after the fault clearing (s)	Re-sim RAS (MW)	Adapt. RAS (MW)
0.1	2250	2300
0.11	2250	2400
0.12	2300	2400
0.13	2350	2500
0.14	2400	2600
0.15	2450	2600
0.16	2500	2700
0.17	2550	2800
0.18	2600	2900
0.19	2650	3000
0.19	2750	3100
0.20	2800	3200

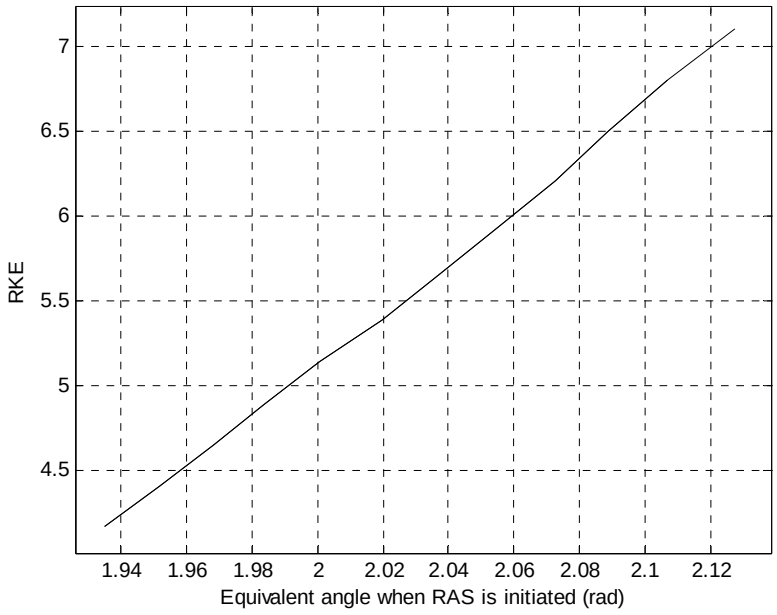

Figure 4.17 *RKE* vs. equivalent angle when the RAS is initiated

4.3 Discussion

The proposed RAS computation method calculates the *DPE*, the approximate ability of each RAS action to increase the stability of the system, and the *RKE*, the energy margin of an unstable case following a RAS action, based on transient energy analysis. A RAS action can be determined directly by comparing the *DPE* and *RKE* instead of by repeated time domain simulations. We observed the following:

- The calculated *DPE* can be reused for different operating points and fault locations for the specific MOD and the given post-fault network topology. To calculate the RAS amount for a new unstable case, one only needs to calculate the *RKE*. The

proposed method can reduce the computational burden compared with the repeated time domain simulation.

- The proposed method is adaptive to operating points and fault locations on the tie lines.
- The proposed method is also adaptive to different fault clearing time and RAS initiation time. This suggests the effect of communication delay can be included in the proposed computation procedure.
- The proposed method is robust to RAS location and variable critical cases.
- The examples in this chapter illustrate the clarified near linear relationships of *RKE* with different variables, such as different transfer power (or operating points), fault location, different RAS time and different fault clearing time. *DPE* also has a near linear relationship with the transfer power. These near linear relationships can be used to determine the RAS amount for cases that are not simulated; hence, the computation burden is further reduced.

Chapter 5

REAL-TIME TRANSIENT INSTABILITY DETECTION FOR RAS

5.1 Triggering RAS based on decision tree

5.1.1 Decision trees

A decision tree (DT) is a classifier that is built off-line in the shape of a top-down tree using a training data set of examples. The performance of a DT is evaluated by the classification errors when the tree is tested on unseen test sets of examples. Each example in the training and test sets includes an input vector and its correct classification (e.g., stable or unstable). The classifying procedure for a new input starts from the top node, i.e., the root of the tree, until it reaches a terminal node. Each node represents a decision rule that splits the cases into subsets. The tree's depth can be defined as the maximum number of nodes that must be visited before reaching a terminal node. In this work, the DTs are built using the open source software package C4.5 [15]. The default parameters provided by the software are used. The criterion for the decision rules used were to maximize the net information gain, i.e., entropy, from the splitting of the data. After the full tree is trained, C4.5 prunes to avoid over-fitting the data.

5.1.2 Triggering RAS

As defined in [6], a RAS is designed to detect abnormal system conditions and take predetermined corrective action to preserve system integrity and provide acceptable system performance. RAS tend to be system and situation specific. For transient instability, the RAS needs to counteract the instability in a specific MOD.

The measurements of a PMU are synchronized based on the GPS so that the measured phasor angles from dispersed locations in a power system can be compared on a common time reference axis [29] in both the steady-state and following a disturbance. It has been illustrated in [32-33] that decision trees can predict instability of power system with high accuracy using real-time phasor measurements as input. Similarly, it is possible to implement the adaptive trigger of RAS based on decision tree and phasor measurements. Considering that the RAS tends to be MOD specific, the classification of the decision tree needs to contain the MOD information. Two classifications are used here: “Unstable in MOD” and “Not unstable in MOD” (which includes stable and unstable cases in other MODs). If the decision tree detects Unstable in MOD, the RAS that counteracts the instability in the specific MOD will be triggered.

5.2 Practical issues for real-time transient instability detection

5.2.1 Time delay in wide area measurement system

Time delay in the wide area measurement system is mainly caused by PMU processing and the communication system. The total delay in the process of measuring and sending data to the control center can be calculated by [45]:

$$\tau_m = \tau_f + \tau_p + \frac{L}{R} + \mu \tag{5.1}$$

where τ_f is the delay associated with transducers, DFT (Discrete Fourier Transform) processing, data concentration and multiplexing. τ_f is variable according to the number of measurements and the length of each measurement. The link propagation delay τ_p is a function of the communication media and the distance. The time delay associated with different communication media can be found in [45]. L is the amount of data transmitted, R is the data rate of the link. The delay expressed by $\frac{L}{R}$ can be negligible for media with high-speed transmission, such as fiber-optic cable. Finally, μ is the associated random delay arising from PMU measurements and communication delays.

Suppose the measurements in a time window of τ_s milliseconds are used to detect the instability. The calculation in the control center needs time τ_c and the communication delay in sending a command to the control equipment is $\tau_p^{'}$. The elapsed time between the fault clearing and the control action is:

$$\tau_r = \tau_s + \tau_m + \tau_c + \tau_p^{'} \tag{5.2}$$

Substituting (5.1) into (5.2) and assume $\frac{L}{R} = 0$, we have

$$\tau_r = \tau_s + \tau_f + \tau_p + \tau_p^{'} + \tau_c + \mu \tag{5.3}$$

The maximum available time to initiate a RAS action after the fault clearing depends on the severity of the contingency and system operating criteria. Suppose the maximum available time is $\tau_r^{\max}$, then we have:

$$\tau_r \le \tau_r^{\max} \tag{5.4}$$

and

$$\tau_s \le \tau_r^{\max} - \tau_f - \tau_p - \tau_p^{'} - \tau_c - \mu \tag{5.5}$$

Now assume $\tau_r^{\max}$ = 200ms [6] and use the typical data given in [45], for example with $\tau_p = \tau_p^{'}$ = 25 ms (fiber-optic cable) and τ_f = 75 ms, then:

$$\tau_s \le 75 - \tau_c - \mu \tag{5.6}$$

Considering τ_c is a comparatively small, the measurements available for instability detection are the measurements obtained within about 4 ~ 4.5 cycles on the fundamental frequency, i.e., 67ms ~ 75ms, after the fault clearing. This is much shorter than $\tau_r^{\max}$, 200ms. Therefore, the time delay in the wide area measurement system is an important factor when determine how many measurements can be used for the instability detection. In the actual wide area measurement systems, the time delay will be different depending on the practical PMU settings and communication media. Communication traffic could also have a significant effect on the time delay [8].

5.2.2 PMU measurements independent of event occurrence

The synchronization of the phasor measurements based on the GPS is independent of the occurrence of the system events. Thus, the time of the first measurement after the

fault clearing is independent of the fault clearing. Assume there are two cycles between two consecutive measurements received at the control center [29, 46]. The first measurement may be the response of the system right after the fault clearing, or at a time between the fault clearing and two cycles later. The number of available measurements for detection will also be affected by the sampling time of the first measurement. For example, suppose the time window for detection is 4 cycles. The available measurements for the detection will be either three measurements, at the 0^{th}, 2^{nd} and 4^{th} cycles, where 0 is for immediately after the fault clearing or two measurements, e.g. at the 1^{st} and 3^{rd} cycles. Therefore, the RAS trigger needs to be designed to use only the first two sets of measurements to function in either situation. Availability of measurements for instability detection is illustrated in Figure 5.1. Robustness of the decision tree to variation in the sampling time of the first measurement needs to be considered.

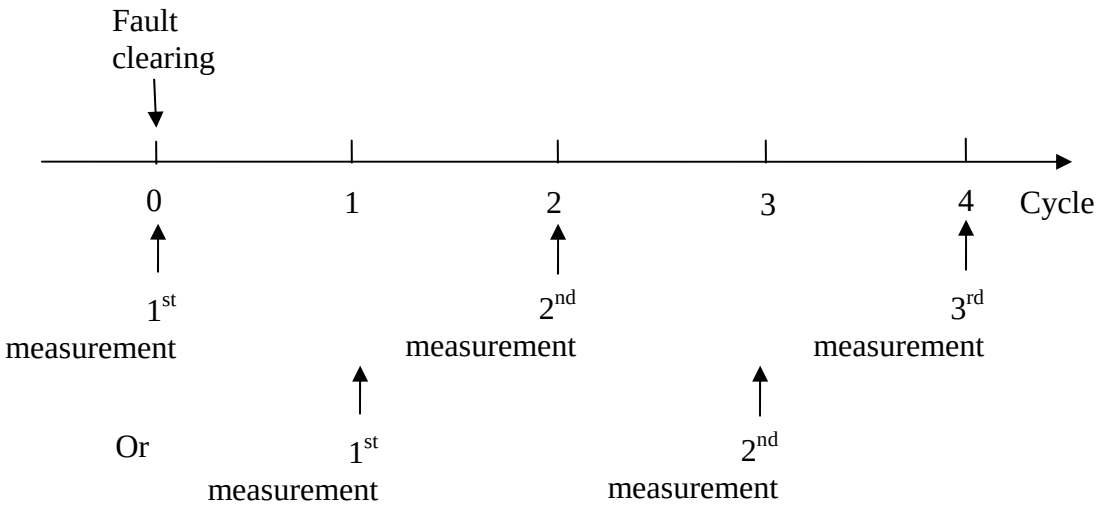

Figure 5.1 Availability of PMU measurements for instability detection

5.2.3 Input features to DT

The inputs to decision tree depend on system conditions and requirements. For example, the timing issues discussed above restrict the number of available phasor measurements. Moreover, the measurements may come from different busses in the system depending on the placements of PMU. In this work, time domain simulations are used to simulate the phasor measurements. We assume there are two cycles between consecutive measurements. The voltage angles of busses instead of the rotor angles of generators are used as the input features since most PMU are installed on the busses in current power system. The angular speed and acceleration may or may not be used as the input features. It depends on how many phasor angles are measured, since in practice the speed and acceleration are obtained from:

$$v = \frac{\delta(1) - \delta(0)}{\Delta t} \tag{5.7}$$

$$acc = \frac{\delta(2) - 2\delta(1) + \delta(0)}{\Delta t^2} \tag{5.8}$$

The decision tree can also take input from phasor magnitudes, system events such as, transmission line trip, and pre-fault power transfers.

5.2.4 Using phasor magnitudes

Phasor magnitudes measured in the transient period may deviate from the real value [32, 47-48]. Still, new signal processing techniques show promise for improved accuracy of the magnitude measurements, so that the control and protection relays may be able to use the phasor magnitudes as direct inputs [47]. One problem with including the phasor

magnitude is that the first measured magnitude after the fault clearing may not be suitable as an input to the decision trees for instability detection. The phasor can be defined as [13]:

$$X = \frac{\sqrt{2}}{N} \sum_{k=1}^{N} x_k e^{-j2k\pi / N} \tag{5.9}$$

where N is the total number of samples in one period, X is the phasor, and x_k is the waveform samples. Considering that synchronization of PMU is independent of the fault clearing, it is possible that the first measured magnitude uses samples before the fault clearing, i.e., the first measured magnitude after the fault clearing is the value of the fault-on system instead of the post-fault system. One can use the second measurement after the fault clearing in the detection to avoid using the phasor magnitude value of the fault-one system. The cost of waiting for the subsequent measurement is a delay in how quickly instability can be detected.

5.3 Simulations on IEEE 39-bus system

5.3.1 Study system and simulation method

The modified IEEE 39-bus system from Chapter 4 that is a two-area system along with tie lines from bus 16 to bus 15 and 17 is used. A severe contingency, e.g. 3-phase to ground short circuit fault on the tie lines, may cause the system separate into two groups along the tie lines in the first swing. RAS is needed to avoid the separation by tripping generation and shedding load in the supply and demand areas, respectively. Decision trees based on PMU measurements will be used as the trigger for the RAS. The

classifications of the decision tree are two: unstable in the MOD or not unstable in the MOD. The MOD is as before where the system separates into two groups along the ties.

The training and test data are sampled from the results of the time domain simulations on different operating points and fault scenarios. The operating points are created by randomly adjusting the generation and load on both sides of the ties. Faults on ties and on other randomly selected lines are simulated. Faults may be located at either end or other points on the selected transmission lines. Different fault clearing times are used for each fault location.

The classification of the training and test data can be obtained from the following procedure:

1) Run time domain simulation for the given operating points and fault scenarios. Simulation of 3 seconds is adequate to determine the stability for this test system.
2) If the difference between the angles of any two generators exceeds some limit, say 360 degrees, then the system is unstable, go to step 3. Otherwise, the system is stable, go to step 5.
3) If the difference between the angles of any two generators in the same area exceeds some limit, again say 360 degrees, then the system is unstable but not in the specific MOD of interest, go to step 5. Otherwise, go to step 4.
4) Classify the cases that are unstable in the specific MOD as unstable in MOD.
5) Classify the cases that are stable or unstable but not in the specific MOD as Not Unstable in MOD.

5.3.2 Training and test set creation

For the given two-area system, it has been observed that using pre-fault transfer power as an input feature can improve the performance of decision trees. Hence, the input vectors of all decision trees present in this dissertation will include the pre-fault transfer power. A training set contains a number of cases from different operating conditions (given an operating point and a fault scenario). PMU data that are sampled from the same operating condition but at different sampling time can be included as one or two examples. As discussed in Section 5.2.2, the PMU synchronization is independent of event occurrence so that one needs to evaluate the robustness of DT to variation of the sampling start time. Including two examples for each operating conditions in the training and test sets has been used in [32] to increase the robustness. This will be investigated further in the following studies. Figure 5.2 illustrates two different ways to use the PMU data in training set, where $A_{i,Bj}$ is the PMU data at bus j, sampled at i^{th} cycle.

One example for each operating condition

$$\cdots \quad \cdots \quad A_{1,B1} \; A_{1,B2} \; A_{1,B3} \quad A_{3,B1} \; A_{3,B2} \; A_{3,B3} \quad \cdots \quad \cdots$$

Two examples for each operating condition

$$\cdots \quad \cdots \quad A_{1,B1} \; A_{1,B2} \; A_{1,B3} \quad A_{3,B1} \; A_{3,B2} \; A_{3,B3} \quad \cdots \quad \cdots$$

$$\cdots \quad \cdots \quad A_{2,B1} \; A_{2,B2} \; A_{2,B3} \quad A_{4,B1} \; A_{4,B2} \; A_{4,B3} \quad \cdots \quad \cdots$$

Figure 5.2 PMU data sampled at different times in training set

Table 5.1 lists the decision trees and training sets that will be studied. In the column of PMU locations, G is for generator bus and B is for boundary bus (bus15, 16, 17 in this studied system). The sampling time is expressed by n^{th} cycle after the fault clearing, where 0 is immediately following fault clearing. The column of example numbers indicates how many examples for the same operating condition are contained in a training set. For instance, the training sets of decision trees A1~A3 use one example for each operating condition, B1~B3 use two examples and so on. An example may include measurements sampled at different sampling times. If two or more examples are used for the same operating condition, the sampling time of different examples are separated by a semicolon. Similarly, Table 5.2 gives the test sets. Test set 1 uses the same sampling time as the corresponding training set. Test set 2 uses multiple examples to evaluate the robustness to variation in the sampling start time. The data of the training set and the test set are sampled from 4440 and 6480 operating conditions, respectively, for the IEEE 39-bus system study.

As analyzed in subsection 5.2.1, the time delay will reduce the number of the measurements available for instability detection. The effect of time delay can be reflected by using different numbers of measurements. For example, trees A1~A3 and B1~B3 are designed to make the detection based on the first measurement; trees C1~C3 and D1~D3 use the first two measurements and the sampling window is 4 cycles; trees E1~E3 and F1~F3 use three measurements in a 6-cycle sampling window while assuming the first measurement occurs in the first 2-cycle time window after the fault clearing. From (5.7) and (5.8), the angular speed and acceleration may or may not be available depending on the number of phasor angle measurements.

Table 5.1 Training sets

DT	Training set				
	PMU location	Example numbers	Sampling time	Angular speed	Accele-ration
A1	G	1	0	No	No
A2	G and B	1	0	No	No
A3	B	1	0	No	No
B1	G	2	0; 2	No	No
B2	G and B	2	0; 2	No	No
B3	B	2	0; 2	No	No
C1	G	1	0, 2	Yes	No
C2	G and B	1	0, 2	Yes	No
C3	B	1	0, 2	Yes	No
D1	G	2	0, 2; 2, 4	Yes	No
D2	G and B	2	0, 2; 2, 4	Yes	No
D3	B	2	0, 2; 2, 4	Yes	No
E1	G	1	0, 2, 4	Yes	Yes
E2	G and B	1	0, 2, 4	Yes	Yes
E3	B	1	0, 2, 4	Yes	Yes
F1	G	2	0, 2, 4; 2, 4, 6	Yes	Yes
F2	G and B	2	0, 2, 4; 2, 4, 6	Yes	Yes
F3	B	2	0, 2, 4; 2, 4, 6	Yes	Yes

Table 5.2 Test sets

DT	Test set 1		Test set 2	
	Example Numbers	Sampling time	Example Numbers	Sampling time
A1-A3	1	0	3	0; 1; 2
B1-B3	2	0;2	3	0; 1; 2
C1-C3	1	0, 2	3	0, 2; 1, 3; 2, 4
D1-D3	2	0, 2; 2, 4	3	0, 2; 1, 3; 2, 4
E1-E3	1	0, 2, 4;	3	0, 2, 4; 1, 3, 5; 2, 4, 6
F1-F3	2	0, 2, 4; 2, 4, 6	3	0, 2, 4; 1, 3, 5; 2, 4, 6

5.3.3 Decision trees based on phasor angles

Table 5.3 shows the evaluation for decision trees based on phasor angles and pre-fault transfer power. The performance of the decision trees are indicated by the percentage of inputs that are correctly classified. For example, the number in the column "Unstb. in MOD" indicates the percentage of the cases actually unstable in the specific MOD that were correctly classified. Observations from Table 5.3 are summarized in the following:

1) Using only the phasor angles of generator busses, the performance is not adequate (trees A1, B1).
2) By including phasor angles of the boundary buses, the performance is significantly improved (trees A2~A3 and B2~B3).
3) Using the angular speed or acceleration can improve the performance on test set 1; however, it may cause the decision trees to be sensitive to variations in the first sampling time (compare the performance of trees C1~C3 and E1~E3 on test

sets 1 and 2). Using training sets with two examples only can improve the robustness (trees D1~D3 and F1~F3).

4) Instability can be detected in a very short time window (e.g., trees A2~A3 use the first measurement after the fault clearing). Using a longer sampling window and more measurements does not guarantee a better performance.

Table 5.3 DT evaluation including angles, speed and acceleration (IEEE 39-Bus)

DT	Nodes	Depth	Test set 1		Test set 2	
			Unstb. in MOD	Not unstb. in MOD	Unstb. in MOD	Not unstb. in MOD
A1	175	10	86	96	88.8	94.5
A2	95	10	96.2	99.2	95.5	98.1
A3	75	11	95.5	99	95.6	97.2
B1	263	15	89.5	95.7	87.9	95.9
B2	155	10	96	99.2	95.1	99.2
B3	139	14	93.4	99	93.2	98.9
C1	93	9	95.3	97.5	77.1	92.8
C2	69	8	97.7	99.6	92.2	98.1
C3	73	9	97.3	99.4	96	98.2
D1	171	14	95	99	91.9	98.7
D2	129	12	97.1	99.5	95.8	99.6
D3	149	13	96.1	99.5	93.6	99.6
E1	85	11	96.6	99	85.2	94.2
E2	61	8	97.5	99.3	93.5	97.7
E3	65	11	97.9	99.5	88.3	97.2
F1	123	12	96.2	98.9	94.2	98.9
F2	113	10	97	99.4	96	99.4
F3	133	12	96.1	99.6	94.7	99.5

Table 5.4 DT evaluation including angles only (IEEE 39-Bus)

DT	Nodes	Depth	Test set 1		Test set 2	
			Unstb. in MOD	Not unstb. in MOD	Unstb. in MOD	Not unstb. in MOD
C1	143	11	86.8	95.9	88.5	94
C2	85	10	95.7	99.1	95.1	98.1
C3	81	10	95.7	98.9	95	97.3
D1	233	14	90.3	95.2	89.9	95.2
D2	147	12	95.3	99.2	94.2	99.1
D3	151	15	93.2	99.5	92.1	99.5
E1	133	12	91.4	95.6	91.5	95.3
E2	85	9	96.6	99.4	96.2	98.4
E3	91	11	97	99.5	95.2	98.6
F1	185	14	92.7	95.9	92.8	95.9
F2	121	11	95.9	99.5	95.7	99.5
F3	145	12	96.5	99.4	96.4	99.3

Decision trees that are similar to C1~F3 except for excluding the speed and acceleration in the input are also studied. Table 5.4 shows the results. These trees are robust to the variation in the sampling start time. Note the decision trees still use the notations C1~F3, but do not include angular speed and acceleration as input.

5.3.4 Decision trees using phasor magnitudes

Table 5.5 shows the results of the DTs that include the voltage magnitudes as input. The voltage magnitudes are sampled together with the phasor angles. It is observed from the evaluation on test set 1 that using voltage magnitudes can improve the detection accuracy; however, from the evaluation on test set 2, it is noticed that the voltage magnitudes causes the decision trees to be sensitive to variation in the sampling time of

the first measurement. The tie line currents can also be used as inputs to the decision trees. Results using these currents are shown in Table 5.6. It is seen that the instability detection has improved and that detection is robust to the variation in the sampling time of the first measurement.

Table 5.5 DT evaluation including voltage magnitudes (IEEE 39-Bus)

DT	Nodes	Depth	Test set 1		Test set 2	
			Unstb. in MOD	Not unstb. in MOD	Unstb. in MOD	Not unstb. in MOD
A1	75	10	93.5	99.0	63.9	99.2
A2	84	11	95.3	99.1	76.3	97.5
A3	73	9	96.3	99.3	92	97.8
B1	181	13	94.0	98.7	91.1	98.8
B2	127	11	95.5	99.5	94	99.3
B3	127	12	95.2	99.5	94.3	99.4
C1	81	10	93.3	98.7	71.7	99
C2	75	11	94.7	99.3	73	97.8
C3	81	9	95.1	99.4	92	98.4
D1	161	14	95.3	99	93.7	99
D2	125	14	96.2	99.5	94.8	99.5
D3	129	12	95.3	99.6	94.9	99.5
E1	83	11	95.2	99.3	72.9	98.7
E2	79	12	95.8	99.4	81.7	97.8
E3	75	10	95.8	99.4	93.8	98.3
F1	145	13	95.7	99.1	95.6	99.1
F2	117	14	95.7	99.3	95.1	99.3
F3	121	14	95.9	99.3	95.1	99.3

Table 5.6 DT evaluation including tie line currents (IEEE 39-Bus)

DT	Nodes	Depth	Test set 1		Test set 2	
			Unstb. in MOD	Not unstb. in MOD	Unstb. in MOD	Not unstb. in MOD
A1	83	12	96.7	98.5	97.6	96.4
A2	75	11	97	98.8	97.6	97.1
A3	81	11	96.3	98	97.2	96.1
B1	149	17	94.8	99.1	93.9	99.1
B2	145	13	95.3	99	94.5	99
B3	143	12	94.9	99.3	93.6	99.2
C1	81	13	96.8	98.8	97.8	96.7
C2	77	12	96.7	98.7	96.4	97.2
C3	83	13	95.6	98.8	95.7	97
D1	135	14	94.6	99.1	93.7	99.1
D2	137	14	94.6	99.4	93.3	99.4
D3	145	12	94.9	99.4	93.6	99.3
E1	87	12	97	98.8	97.8	96.9
E2	77	12	96.9	98.9	97.8	97.1
E3	83	11	97.2	98.5	97.5	96.5
F1	137	11	95.1	99	94.8	98.9
F2	131	12	95.5	99.1	94.5	99.1
F3	137	11	95.5	99.4	94.4	99.3

Results including the 2nd measurement are presented in Table 5.7 where the decision trees H1~H3 are similar to the decision trees A1~A3 in the Table 5.6, except the training sets use the example at the 2nd cycle after the fault clearing. Similarly, test set 1 uses the example at the 2nd cycle and test set 2 uses examples at 2nd, 3rd and 4th cycles after fault clearing.

Table 5.7 DT evaluation including 2nd measurement of tie line current (IEEE 39-Bus)

DT	Nodes	Depth	Test set 1		Test set 2	
			Unstb. in MOD	Not unstb. in MOD	Unstb. in MOD	Not unstb. in MOD
H1	81	10	96.8	99.1	97.8	97.1
H2	81	10	97.3	99.1	98.1	97.1
H3	85	13	96.2	99	97.4	96.9

5.3.5 System events as discrete inputs

System events can be used by decision trees as a discrete input feature, or as prior knowledge, e.g., only using the data associated with the specific event to train and test the decision trees. Here, the system event, a tie line between bus 16 and 17 tripping, is studied. Table 5.8 illustrates the evaluation results on test set 2. The training and test sets are identical to those defined in Table 5.1 and 5.2, except for including the system event in the input vector. The notation for the DTs are the same as used in the previous section. It is observed that this additional information slightly improves the performance of the decision trees A1~D3.

5.3.6 Hard detection

The typical trigger logic of an event-based RAS using hard detection could be as following:

1) Arm if the transfer power on tie lines is greater than a predefined threshold.
2) Initiate if the tie lines are tripped and the RAS has been armed.

Table 5.9 shows the results from hard detection again evaluated on the test set that is created in subsection 5.3.4 and using the system event as an input. Using 960 MW as the

threshold, 100% accuracy of detection on ‘Unstable in MOD’ can be obtained; however, for the class of ‘Not Unstable in MOD’, the detection accuracy is 36%. Clearly, the decision trees based on the real time phasor measurements detect the instability with far greater precision and robustness.

Table 5.8 DT evaluation on test set 2 including system event (IEEE 39-Bus)

DT	Event is an input feature			Event is a prior knowledge		
	Depth	Unstb. in MOD	Not unstb. in MOD	Depth	Unstb. in MOD	Not unstb. in MOD
A1	10	93.7	97.7	9	95.6	94.7
A2	10	97	97.8	9	97.2	94.2
A3	10	95.6	98	10	97.4	92
B1	10	92.1	98.7	10	94.3	96.5
B2	12	95	99.2	10	96.2	97.2
B3	12	91.8	99.6	10	94.9	97.8
C1	10	94.3	97.6	8	97.1	93.2
C2	10	96.7	97.9	8	97.4	93.1
C3	10	97.5	97.5	8	98.6	89.3
D1	10	93.2	99	10	97	96.4
D2	11	95.3	99.3	9	98.2	97.1
D3	13	95.2	99.3	10	97.4	97.2
E1	13	84.3	95.8	11	78.7	98.7
E2	12	91.8	99.2	10	92.3	85.3
E3	9	88.8	97.1	7	85.9	96.5
F1	13	96.6	99.4	8	97	97.6
F2	10	95.8	99.4	8	97.9	97.3
F3	11	94.2	99.7	10	96.9	97.9

Table 5.9 Results from hard detection

Threshold of transfer power (MW)	Unstb. in MOD (%)	Not unstb. in MOD (%)
960	100	36
1050	79.8	95.4

5.4 Simulations on WECC 179-bus system

Decision trees are used for transient instability detection on the WECC 179-bus that was analyzed in Chapter 4. Along the transmission path from bus 76 to 82, the system is configured as a two-area system. North of bus 76 is the primary supply area that includes six generators at busses 30, 35, 65, 70, 77 and 79. The system is weakened by stretching the transmission lines between bus 76 and 82, so that two line outages may be severe enough to separate the system into two groups along this transmission path in the first swing.

The decision trees are created and evaluated by the same method as used for the IEEE 39-bus system. The data of the training set and the test set are sampled from 9793 and 10284 operating conditions, respectively. Table 5.10 shows the results for the decision trees whose inputs are the phasor angles and the tie currents of the first measurements after the fault clearing. Similar to the study on IEEE 39-bus system in Section 5.3, these decision trees are denoted A1~A3. Table 5.11 shows the evaluation results of the decision trees similar to Table 5.10 except the system events are included. Comparing these two tables, it is observed that for the WECC 179-bus system, the system event of tripping the tie lines improves the accuracy of the instability detection.

Table 5.10 DT evaluation including angles and tie line currents (WECC 179-Bus)

DT	Nodes	Depth	Test set 1		Test set 2	
			Unstb. in MOD	Not unstb. in MOD	Unstb. in MOD	Not unstb. in MOD
A1	341	24	83.5	92.8	84.6	91.9
A2	315	18	86.9	88.2	87.9	87.2
A3	317	24	89.7	88.8	90.3	88.2

Table 5.11 DT evaluation including event, angles, and tie line currents (WECC 179-Bus)

DT	Nodes	Depth	Test set 1		Test set 2	
			Unstb. in MOD	Not unstb. in MOD	Unstb. in MOD	Not unstb. in MOD
A1	17	5	97.5	83.6	97.5	82.4
A2	17	5	97.5	83.6	97.5	82.4
A3	29	6	98.1	91.5	97.9	90.5

Table 5.12 DT evaluation including 2nd measurement of angles and tie line currents

(WECC 179-Bus)

DT	Nodes	Depth	Test set 1		Test set 2	
			Unstb. in MOD	Not unstb. in MOD	Unstb. in MOD	Not unstb. in MOD
H1	297	21	88	93.7	88.5	93.6
H2	327	18	88.3	69.9	88.5	71.2
H3	257	19	87.2	89.4	87.9	89

Table 5.13 DT evaluation including event , 2nd measurement of angles and tie line currents (WECC 179-Bus)

DT	Nodes	Depth	Test set 1		Test set 2	
			Unstb. in MOD	Not unstb. in MOD	Unstb. in MOD	Not unstb. in MOD
H1	17	5	97.5	83.7	97.5	83.2
H2	17	5	97.5	83.7	97.5	83.2
H3	31	6	97.7	92	97.6	91.6

Table 5.14 Hard detection (WECC 179-Bus)

Threshold of transfer power (MW)	Unstb. in MOD (%)	Not unstb. in MOD (%)
1700	100	15.69
1900	99.48	51.43
1985	88.93	66.30
2000	82.19	78.44

Including inputs of the phasor angles and the tie currents as the second measurements after the fault clearing is evaluated in Table 5.12 and Table 5.13, where the decision trees are denoted as H1~H3. It is seen that transient instability can be detected with high accuracy even when using only a short time window. For comparison, Table 5.14 shows the hard detection results on the same test sets as used in Table 5.11. It can be seen that the decision trees can provide better detection of transient instability.

5.5 Discussion

This chapter introduces the concept of an adaptive trigger for RAS using the instability detection based on phasor measurements. Specifically, given a two-area

system model, decision trees based on the phasor measurements are used to detect the transient instability in the specific MOD where the system separates into two groups along the ties. A RAS action for this specific MOD will be triggered if the instability is detected. Effects of practical issues on the performance of the decision trees are also studied. The study results are summarized as following:

- Communication and measurement time delays reduce the number of available phasor measurements for instability detection.
- Instability can be detected in a very short time window with high accuracy.
- Using phasor measurements in a longer sampling window does not improve the instability detection.
- Robustness of the detection to variation in the sampling time of the first measurement needs to be evaluated. Using angular speed, acceleration and voltage magnitude as inputs tends to lead to more sensitive performance of the DT.
- Using tie currents as input can improve the performance and these DTs are robust to the variation in the sampling time of the first measurement.
- For a two-area system with the MOD separating the system along the ties, phasor angles of the boundary buses improve the performance.
- System events can be used as input features. For a large complex system, using knowledge of the system events can greatly improve detection.

Chapter 6

CONCLUSIONS AND FUTURE WORKS

6.1 Conclusions

A new method for adaptive RAS has been proposed. Given a two-area system model and the MOD that the system will separate into two areas along the ties after a severe fault on the ties, the proposed method uses the critical case, generally the case reaching the transfer limit, as the intermediary for RAS calculation. This method separately calculates *DPE* and *RKE* with respect to the critical case. The *DPE* is the capability to absorb excess kinetic energy of the cases having less transfer power than the critical case has. The *RKE* is the residual corrected kinetic energy of the unstable cases following a fictitious RAS action that reduces the transfer power to the level of the critical case. The *DPE* are calculated first and can be reused for the given system topology and the mode of disturbance. For an unstable case, one only needs to run time domain simulation once to calculate its *RKE* with respect to the critical case. Then a sufficient RAS action can be determined by comparing the *RKE* and the *DPE*. Hence, the repeated time domain simulation can be avoided and the computational burden will be reduced.

For the given system topology and the specific MOD, the proposed method is adaptive to different operating points and different fault locations on the tie lines. It is also adaptive to different fault clearing time and RAS initiation time. It is robust to the

variable locations of the RAS actions and the variations of the critical cases. Communication delay also can be included in the proposed computation procedure. The approach can be used in the off-line computation to replace the conventional repeated time domain simulation in the RAS design. This also enables us to establish an adaptive RAS using fast on-line computation from readily available.

A new transient energy calculation method based on the EPEA curve of the equivalent OMIB system has been proposed to support the proposed adaptive RAS calculation method. The change of the transient energy with RAS action can be clearly observed and easily calculated on the EPEA curve. It is especially suitable for transient energy calculation in the situations with varying mechanical power, such as generation rejection. The concept of hybrid transient stability analysis is used to calculate all transient energy assuming the MOD is not changed by the RAS action. The method is flexible with respect to system modeling. The effectiveness and robustness of the proposed methods for the adaptive RAS and transient energy calculation have been evaluated on IEEE 39-bus and WECC 179-bus systems.

Transient instability detection based on decision tree and phasor measurements are designed as the trigger of RAS actions. Specifically, given a two-area system model, decision trees classify whether a scenario is unstable in a particular MOD where the system will separate into two groups along the tie lines. A RAS action for this specific MOD will be triggered if the instability with the same MOD is detected. The effects of the practical issues on the performance of the decision trees have been studied on the IEEE 39-bus and the WECC 179-bus systems.

The simulation results show that the decision trees can use the phasor angles measured right after the occurrence of system event to detect the transient instability with high accuracy. Because of the fast detection capability of the decision trees, the time delay associated with PMU measurement and communication system will not have significant effect on the detection of instability, although the time delay may reduce the number of the available measurements for the detection. The decision trees taking input from angular speed and acceleration and voltage magnitude may be sensitive to variation in the sampling time of the first PMU measurement. For the two-area system model and the specific MOD, using the phasor angles of the boundary busses and the tie currents as input can improve the performance of the decision trees. At the same time, the decisions are robust to the variation of the sampling time of the first measurement. For a large complex system, knowledge of the system events can greatly improve detection The numerical results show that the decision trees have promise to implement the adaptive trigger for a RAS based on both system event and the consequent phasor measurements.

6.2 Future works

Practical use of the developed methods requires several further considerations beyond the work in this dissertation. Specifically:

1) In the real-time transient instability detection, new detection rules can be established based on both of the decision trees and experience. It may be possible to improve the accuracy of the detection for the unstable cases and the use of such experience may allow for faster acceptance of the techniques.

2) A number of communication and signal processing events have not been full investigated here. These include susceptibility to noise and lost measurement. Practical implementations must be robust to such eventualities.
3) The fundamental assumption in this work is that the RAS is effective in only a specific MOD for a two area system. The two area limitation can probably be extended easily or rather merely at the cost of increased computations. On the other hand, a given system may have several MOD of interest and numerous RAS implementations. It is critical that these operate without interference or in a coordinated manner.

BIBLIOGRAPHY

[1] G. T. Heydt, C. C. Liu, A. G. Phadke, V. Vittal, "Solution for the Crisis in Electric Power Supply," *IEEE Computer Application in Power*, Vol. 14, No. 3, pp. 22-30, July 2001.

[2] M. La. Scala, M. Trovato and C. Antonelli, "On-line Dynamic Preventive Control: An Algorithm for Transient Security Dispatch," *IEEE Trans. on Power Systems*, Vol.13, No. 2, pp. 601-610, May 1998.

[3] A. A. Fouad and J. Tong, **"**Stability Constrained Optimal Rescheduling of Generation," *IEEE Trans. on Power Systems*, Vol. 8, No. 1, pp. 105-112, Feb. 1993.

[4] D. Ruiz-Vega and M. Pavella, "A Comprehensive Approach to Transient Stability Control. I. Near Optimal Preventive Control," *IEEE Trans. on Power Systems*, Vol. 18, No. 4, pp. 1446-1453, Nov. 2003.

[5] W. Li and A. Bose, "A Coherency Based Rescheduling Method for Dynamic Security," *IEEE Trans. on Power Systems*, Vol. 13, No. 3, pp. 810- 815, Aug. 1998.

[6] "System Protection Schemes in Power Networks," *CIGRÉ report, Task Force 38.02.19*, Jun 2001.

[7] G. Trudel, S. Bernard, G. Scott, "Hydro-Quebec's defense plan against extreme contingencies," *IEEE Trans. on Power Systems*, Vol. 14, No. 3, pp. 958 – 965, Aug. 1999.

[8] K. Tomsovic, D. Bakken, V. Venkatasubramanian and A. Bose, "Designing the Next Generation of Real-Time Control, Communication and Computations for Large Power System," *Proceedings of the IEEE*, Vol. 93, No. 5, pp. 965-979, May 2005.

[9] P. Kundur, "Power System Stability and Control", McGraw Hill, 1996

[10] C. Taylor, “Power System Voltage Stability”, McGraw Hill, 1996

[11] North America Reliability Corporation, Reliability Standards for the Bulk Electric Systems of North America, http://www.nerc.com/~filez/standards/Reliability_Standards.html

[12] I. Kamwa, R. Grondin and Y. Hebert, “Wide-area Measurement Based Stabilizing Control of Large Power Systems -- a Decentralized/Hierarchical Approach,” *IEEE Trans. on Power System*s, Vol. 16, No. 1, pp. 136-153, Feb. 2001.

[13] California ISO, “Transmission Economic Assessment Methodology (TEAM), ” Available www.caiso.com/docs/2003/03/18/2003031815303519270.html

[14] California ISO, “ISO Grid Planning Standards,” Available www.caiso.com/docs/09003a6080/14/37/09003a608014374aex.html

[15] Open source software of decision tree, “C4.5 Tutorial,” www2.cs.uregina.ca/~hamilton/courses/831/notes/ml/dtrees/c4.5/tutorial.html

[16] A. A. Fouad and V. Vittal, “Power System Transient Stability Analysis Using Transient Energy Function Method,” Prentice Hall, 1990.

[17] A. A. Fouad, A. Ghafurian, K. Nodehi and Y. Mansour, "Calculation of Generation-Shedding Requirements of the B.C.Hydro System Using the Transient Energy Function," *IEEE Trans. on Power System*s, Vol. PWRS-1, No.2, pp. 17-24, May 1986.

[18] Y. Mansour, E. Vaahedi, A. Y. Chang, B. R. Corns, B. W. Garrett, K. Demaree, T. Athay and K. Cheung, “B.C.Hydro’s On-line Transient Stability Assessment (TSA) Model Development, Analysis, and Post-processing,” *IEEE Trans. on Power Systems*, Vol. 10, No.1, pp. 241–253, Feb. 1995.

[19] H. Ota, Y. Kitayama, H. Ito, N. Fukushima, K. Omata, K. Morita, and K. Kokai, “Development of Transient Stability Control System (TSC System) Based on On-line Stability Calculation,” *IEEE Trans. on Power Systems*, Vol. 11, No. 3, pp. 1463–1472, Aug. 1996.

[20] Y. Fang and Y. Xue, “An On-line Pre-decision Based Transient Stability Control System for the Ertan Power System,” In *Proc. 2000 Power System Technology*, pp. 287-292.

[21] D. Ruiz-Vega and M. Pavella, “A Comprehensive Approach to Transient Stability Control. II. Open Loop Emergency Control,” *IEEE Trans. on Power Systems*, Vol. 18, No. 4, pp. 1454-1460, Nov. 2003.

[22] J.A. Huang, G. Vanier, A. Valette, S. Harrison, and L. Wehenkel, “Application of data mining techniques for automat settings in emergency control at Hydro-Qudbec,” *Power Engineering* Society *General Meeting, 2003, IEEE*, Vol. 4, pp. 2037-2044, 13-17 July, 2003.

[23] Y. Zhang and K. Tomsovic, "Adaptive Remedial Action Scheme based on Transient Energy Analysis," *Proceedings of the 2004 Power Systems Conference & Exposition (PSCE)*, Oct. 2004, New York, pp. 1326 - 1332.

[24] Y. Zhang and K. Tomsovic, “Remedial Action Scheme based on fast transient energy calculation using the curve of equivalent power versus equivalent angle,” Submitted to *Int. Journal of Electrical Power and Energy Systems*.

[25] Y. Zhang and K. Tomsovic, "Adaptive Remedial Action Scheme Based on Fast Calculation of Transient Energy," Submitted to *IEEE Trans. on Power Systems*.

[26] Y. Xue, T. Van Cutsem and M. Ribbens-Pavella, “A Simple Direct Method for Fast Transient Stability Assessment of Large Power Systems,” *IEEE Trans. on Power Systems*, Vol. 3, No. 2, pp. 400-412, May 1988.

[27] Y. Zhang, L. Wehenkel, P. Rousseaux, and M. Pavella, “SIME: A hybrid approach to fast transient stability assessment and contingency selection,” Int. Journal of Electrical Power and Energy Systems, vol. 19, no.3, pp. 195–208, 1997.

[28] L. Wehenkel, “Automatic Learning Techniques in Power Systems,” Kluwer Academic Publishers, 1997.

[29] A. G. Phadke, “Synchronized phasor measurements-a historical overview,” *Transmission and Distribution Conference and Exhibition 2002: Asia Pacific. IEEE/PES*, Vol. 1, 6-10 Oct. 2002, pp. 476 – 479.

[30] V. Centeno, A. G. Phadke, A. Edris, "Adaptive Out-Of-Step Relay with Phasor Measurement," *Sixth International Conference on Developments in Power System Protection, 25-27th March 1997*, pp. 210-213.

[31] G. Karady and J. Gu, "A Hybrid Method for Generation Tripping," *IEEE Trans. on Power Systems*, Vol. 17, No. 4, pp. 1102-1107, Nov. 2002.

[32] S. Rovnyak, S. Kretsinger, J. Thorp and D. Brown, "Decision Trees for Real-time Transient Stability Prediction," *IEEE Trans. on Power Systems*, Vol. 9, No. 3, pp. 1417-1426, Aug. 1994.

[33] R. F. Nuqui, A.G. Phadke, R.P. Schulz and N Bhatt, "Fast On-Line Voltage Security Monitoring Using Synchronized Phasor Measurements and Decision Trees," *IEEE Power Engineering Society Winter Meeting, 28 Jan. - 1 Feb. 2001*, Vol.3, pp. 1347 – 1352.

[34] Y. Zhang and K. Tomsovic, "Real-time Transient Instability Detection Based on Decision Trees Emphasized with RAS," submitted to *IEEE Trans. on Power Systems.*

[35] N. Kakimoto, Y. Ohsawa and M. Hayashi, "Transient Stability Analysis of Large-Scale Power Systems by Lyapunov's Direct Method," *IEEE Trans. on Power Apparatus and Systems*, Vol. PAS 103(1), pp. 160-167, Jan. 1978.

[36] T. Athay, R. Podmore, S. Virmani, "A Practical Method for Direct Analysis of Transient Stability," *IEEE Trans. on Power Apparatus and Systems, Vol. PAS 98, pp. 573-584, 1979.*

[37] H. D. Chiang, F. F. Wu and P. P. Varaiya, "Foundations of the Potential Energy Boundary Surface Method for Power System Transient Stability Analysis," *IEEE Trans. on Circuits and Systems*, Vol. 35, No. 6, pp. 712-728, June 1988.

[38] H. D. Chiang, F. F. Wu and P. P. Varaiya, "A BCU Method for Direct Analysis of Power System Transient Stability," *IEEE Trans. on Power Systems*, Vol. 9, No. 3, pp. 1194-1208, Aug. 1994.

[39] E. Vaahedi, Y. Mansour, A. Y. Chang, B. R. Corns and E. K. Tse, "Enhanced "Second Kick" methods for on-line dynamic security assessment," IEEE Trans. on Power Systems, Vol. 11, No. 4, pp 1976-1982, Nov. 1996.

[40] C. K Tang, C .E. Graham, M. El-Kady and R. T. H.Alden, "Transient Stability Index from Conventional Time Domain Simulation," IEEE Trans. Power Systems, Vol. 9, No. 3, pp.1524–1530, Aug. 1994.

[41] I. A. Hiskens and M. Akke, "Analysis of the Nordel Power Grid Disturbance of January 1, 1997 Using Trajectory Sensitivities", *IEEE Trans. on Power Systems*, Vol. 14, No. 3, pp. 987-994, Aug. 1999.

[42] F.A. Rahimi, M.G. Lauby, J.N. Wrubel and K.L. Lee, "Evaluation of the transient energy function method for on-line dynamic security analysis," *IEEE Trans. on Power Systems*, Vol. 8, No. 2, pp. 497-507, May 1993.

[43] H. Li, G.W. Rosenwald, J. Jung and C.C. Liu, "Strategic Power Infrastructure Defense**,"** *Proceedings of the IEEE*, Vol. 93, NO. 5, May 2005, pp 918-913.

[44] J. Lewis Blackburn, "Protective Relaying Principles and Applications," Marcel Dekker, 1997, Second Edition.

[45] B. Naduvathuparambil, M.C. Valenti, and A. Feliachi, "Communication delays in wide area measurement systems," *System Theory, 2002. Proceedings of the Thirty-Fourth Southeastern Symposium on 18-19 March 2002*, pp.118 – 122.

[46] R. Klump, R. E. Wilson and K. E. Martin, "Visualizing Real-Time Security Threats Using Hybrid SCADA / PMU Measurement Displays," *Proceedings of the 38th Hawaii International Conference on System Sciences – 2005*, pp. 1-9.

[47] G. Benmouyal, E.O. Schweitzer and A. Guzman, "Synchronized phasor measurement in protective relays for protection, control, and analysis of electric power systems," *Protective Relay Engineers, 2004 57th Annual Conference for 30 Mar-1 Apr* 2004, pp.419 – 450.

[48] J. Depablos, V. Centeno, A.G. Phadke and M. Ingram, "Comparative testing of synchronized phasor measurement units," Power Engineering Society General Meeting, 2004. IEEE, 6-10 June 2004, Vol. 1, pp.948 – 954.